PHYSICAL REVIEW D **93,** 054021 (2016)

Z'-induced FCNC decays of top, beauty, and strange quarks

Kaori Fuyuto,[1] Wei-Shu Hou,[2] and Masaya Kohda[3]

[1]*Department of Physics, Nagoya University, Nagoya 464-8602, Japan*
[2]*Department of Physics, National Taiwan University, Taipei 10617, Taiwan*
[3]*Department of Physics, Chung-Yuan Christian University, Chung-Li 32023, Taiwan*

(Received 31 December 2015; published 10 March 2016)

Anomalous $b \to s$ transitions from LHCb data may suggest a new massive gauge boson Z' that couples to the left-handed $b \to s$ current, which in turn implies a coupling to the $t \to c$ current. In this paper, we study flavor-changing neutral current (FCNC) decays of the top quark induced by a Z' boson, namely $t \to cZ'$, based on a model of the gauged $L_\mu - L_\tau$ symmetry (the difference between the muon and tauon numbers) with vectorlike quarks, which was introduced to explain the anomalous LHCb data. We illustrate that searching for $t \to cZ'$ via $Z' \to \mu^+\mu^-$ with LHC Run 1 data can probe a parameter region that is unexplored by B physics for a Z' mass of around $\mathcal{O}(10)$ GeV or greater. We further extend the model to a very light Z' with mass below 400 MeV, which is motivated by the muon $g-2$ anomaly. Taking rare B and K meson decay data into account, we give upper limits on the $t \to cZ'$ branching ratio for the light Z' case, and discuss about its observability at the LHC. We also scrutinize the possibility that the decay $K_L \to \pi^0 Z'$ with $Z' \to \nu\bar{\nu}$ may lead to an apparent violation of the usual Grossman-Nir bound of $\mathcal{B}(K_L \to \pi^0 \nu\bar{\nu}) < 1.4 \times 10^{-9}$.

DOI: 10.1103/PhysRevD.93.054021

I. INTRODUCTION

The measurement of top-quark properties is a major task of the Large Hadron Collider (LHC). In particular, the large amount of $t\bar{t}$ events enables the search for exotic decay modes of the top quark. In line with this, top-quark decays via flavor-changing neutral currents (FCNCs) through the emission of Standard Model (SM) gauge bosons or the Higgs boson have been under intense study by the ATLAS and CMS experiments [1]. In addition, top-quark decays also offer opportunities to directly search for new physics, e.g., a charged Higgs boson (H^+) in $t \to bH^+$ decay [1].

For the down-sector counterpart, the decay properties of bottom quarks, i.e., B mesons, have been thoroughly investigated during the last three decades. So far, in the vast amount of B factory and LHC data, there have been no significant deviations from the SM. From LHC Run 1 data, however, the LHCb experiment has found two tantalizing hints for new physics beyond the SM (BSM) in $b \to s$ transitions. One of these hints is the 3.7σ tension with SM in the angular analysis of $B^0 \to K^{*0}\mu^+\mu^-$ decay, namely, the P_5' anomaly [2,3]. The other is a violation of lepton flavor universality observed in $B^+ \to K^+\ell^+\ell^-$ ($\ell = e$ or μ) decay rates, indicating a 2.6σ discrepancy from the SM prediction, i.e., the R_K anomaly [4]. Though these may be due to statistical fluctuations and/or underestimated hadronic uncertainties, model-independent studies for possible BSM effects have revealed that both the P_5' [5–9] and R_K [10–12] anomalies can be better explained by adding a new contribution to C_9^μ, the Wilson coefficient of the effective operator $(\bar{s}_L\gamma_\alpha b_L)(\bar{\mu}\gamma^\alpha\mu)$. Surprisingly, the required contribution from new physics to C_9^μ for the two anomalies is similar [13,14].

The extra contribution to C_9^μ can be generated by a new massive gauge boson Z' that couples to the muon vector current. In Ref. [15], a Z' model was constructed based on the gauged $L_\mu - L_\tau$ symmetry [16], the difference between the muon and tauon numbers. As an effective theory, the model permits Z' couplings to the SM quark currents through higher-dimensional operators [17]. Reference [15] gave a viable UV-complete model by introducing new vectorlike quarks that mix with SM quarks. The model predicts an effective tcZ' coupling on the same footing, leading to $t \to cZ'$ decay if the Z' is lighter than the top. Such a light Z' is allowed, as it is well hidden with no direct couplings to SM particles with the exception of the muon, the tau, and the associated neutrinos. The $t \to cZ'$ decay, followed by $Z' \to \mu^+\mu^-/\tau^+\tau^-$, opens up a new window to search for the Z' (the $t \to uZ'$ decay with a hadronically decaying Z' was discussed in [18]).

Another phenomenological motivation to introduce the gauged $L_\mu - L_\tau$ symmetry comes from the long-standing $\sim 3\sigma$ discrepancy in the muon anomalous magnetic moment $a_\mu \equiv (g_\mu - 2)/2$ between experimental data and SM predictions [19]. The radiative correction by the Z' loop can provide [20] the right amount of shift, $\Delta a_\mu \sim 3 \times 10^{-9}$, to match with data. However, it was recently found that the Z' effect is severely constrained by the neutrino trident production $\nu_\mu N \to \nu_\mu N\mu^+\mu^-$ process [21]: the good agreement between experimental data and the SM prediction excludes a large portion of the parameter region that could explain the muon $g-2$ anomaly, leaving only the rather light Z' case,

$$m_{Z'} \lesssim 400 \text{ MeV} \quad (\text{muon } g-2). \tag{1}$$

Given this constraint, the muon $g-2$ anomaly and the $b \to s$ transition anomalies cannot be explained simultaneously, as the latter requires a heavy Z' with mass suitably above m_b to generate the contact $(\bar{s}b)(\bar{\mu}\mu)$ interaction for C_9^μ. It is still interesting, though, to investigate connections with the quark currents for the light Z' case that satisfies Eq. (1): the $t \to cZ'$ decay, followed by $Z' \to \mu^+\mu^-$, would exhibit the interesting collider signature of collimated opposite-sign muons from a highly boosted Z'. Moreover, the mass range of Eq. (1) implies that the Z' can be directly produced in B and K meson decays. We have pointed out in Ref. [22] that such a Z' with mass around m_{π^0} can evade $K^+ \to \pi^+ Z'$ searches, but it may cause $K_L \to \pi^0 Z'(\to \nu\bar{\nu})$ with a rate exceeding the commonly perceived Grossman-Nir (GN) bound [23] of $\mathcal{B}(K_L \to \pi^0\nu\bar{\nu}) < 1.4 \times 10^{-9}$. Note that a very light Z' of $L_\mu - L_\tau$ might explain [24] the PeV-scale cosmic neutrino spectrum observed by IceCube [25].

In this paper, we investigate, based on the gauged $L_\mu - L_\tau$ model of Ref. [15], how large the $t \to cZ'$ decay rate can be.[1] We consider the two well-motivated Z' mass ranges: (i) the heavy Z' scenario with $m_b \lesssim m_{Z'} < m_t - m_c$, which is motivated by the $P_5{}'$ and R_K anomalies, and (ii) the light Z' scenario with $m_{Z'} \lesssim 400$ MeV, which is motivated by the muon $g-2$ anomaly. The former was previously sketched in Ref. [15]. It was pointed out that the right-handed tcZ' coupling is unconstrained from B and K meson data and can lead to the $t \to cZ'$ decay with a $\sim$1% branching ratio. We revisit their result by updating $b \to s$ transition data with a correction to the $t \to cZ'$ formula. On the other hand, scenario (ii) was not studied in Ref. [15], but it clearly exhibits rather different phenomenology compared to scenario (i). As the on-shell Z' could be produced by B and K meson decays, the meson decay rates could be hugely enhanced, and even the right-handed tcZ' coupling is constrained by data at the one-loop level. Scenario (ii) is further divided into two categories: (iia) $2m_\mu < m_{Z'} \lesssim 400$ MeV and (iib) $m_{Z'} < 2m_\mu$. In scenario (iib), the Z' decays only into neutrinos, rendering $t \to cZ'$ searches at the LHC difficult, but it gives interesting implications for rare kaon decays as mentioned above.

This paper is organized as follows. We recapitulate in Sec. II the model of Ref. [15], then study $t \to cZ'$ in scenario (i) for a heavy Z' motivated by the $b \to s$ anomalies. We then discuss the observability of $t \to cZ'$ decay at the LHC with $Z' \to \mu^+\mu^-$. In Secs. III and IV, we study $t \to cZ'$ for a light Z' motivated by the muon $g-2$ anomaly. We consider scenario (iia) in Sec. III, where the Z' mass is above the dimuon threshold. We give formulas for FCNC B and K decays, collect relevant rare B and K decay data, then give upper limits on the $t \to cZ'$ branching ratio. In Sec. IV, we consider scenario (iib), where the Z' is below the dimuon threshold. After giving upper limits on $t \to cZ'$ branching ratios, we discuss a special implication for rare kaon decay experiments, expanding the discussion of Ref. [22]. Section V is devoted to discussion and conclusions. In Appendix A, we give the decay distribution for $B^0 \to K^{*0}Z' \to K\pi\mu^+\mu^-$ four-body decay to estimate the efficiency at LHCb, and in Appendix B, we provide the loop functions used in our analysis.

[1] Because of constraints from D meson mixing and decay data, $t \to cZ'$ and $t \to uZ'$ cannot be simultaneously large. We concentrate on the possibilities for large $t \to cZ'$ rates in this paper.

II. P_5'- AND R_K-MOTIVATED Z'

A. Model

We first recapitulate the model introduced in Ref. [15]. A new Abelian gauge group $\mathrm{U}(1)'$ is introduced that gauges the $L_\mu - L_\tau$ symmetry. This $\mathrm{U}(1)'$ symmetry is spontaneously broken by the vacuum expectation value (VEV) of a scalar field Φ, which is charged under $\mathrm{U}(1)'$ but singlet under the SM gauge group. The mass of Z' is given then by $m_{Z'} = g' v_\Phi$, where g' is the $\mathrm{U}(1)'$ gauge coupling and $v_\Phi = \sqrt{2}\langle\Phi\rangle$ is the VEV of Φ. We adopt the convention where the covariant derivative acting on Φ is given by $D_\alpha = \partial_\alpha + ig'\mathcal{Q}'_\Phi Z'_\alpha$, with $\mathcal{Q}'_\Phi = +1$ the $\mathrm{U}(1)'$ charge of Φ. The Z' couples to leptons via

$$\mathcal{L} \supset -g' Z'_\alpha(\bar{\mu}\gamma^\alpha\mu + \bar{\nu}_{\mu L}\gamma^\alpha\nu_{\mu L} - \bar{\tau}\gamma^\alpha\tau - \bar{\nu}_{\tau L}\gamma^\alpha\nu_{\tau L}). \tag{2}$$

We set the kinetic mixing between the $\mathrm{U}(1)'$ and $\mathrm{U}(1)_Y$ gauge bosons to be zero throughout this paper.

In order to induce the effective Z' couplings to the SM quark currents, new vectorlike quarks, which mix with the SM quarks, are introduced: $Q_L = (U_L, D_L)$, U_R, D_R, which replicates one generation of SM quarks, and chiral partners $\tilde{Q}_R = (\tilde{U}_R, \tilde{D}_R)$, $\tilde{U}_L$, $\tilde{D}_L$. Unlike the SM quarks, the new vectorlike quarks are charged under $\mathrm{U}(1)'$, with charges $\mathcal{Q}'_Q = +1$ for $Q \equiv Q_L + \tilde{Q}_R$ and $\mathcal{Q}'_U = \mathcal{Q}'_D = -1$ for $U \equiv \tilde{U}_L + U_R$ and $D \equiv \tilde{D}_L + D_R$. The mass term for the vectorlike quarks is given by

$$-\mathcal{L}_m = m_Q\bar{Q}Q + m_U\bar{U}U + m_D\bar{D}D, \tag{3}$$

where the three mass parameters are taken to be real without loss of generality. The Yukawa mixing term between the vectorlike quarks and SM quarks is given by

$$-\mathcal{L}_{\text{mix}} = \Phi\sum_{i=1}^{3}(\bar{\tilde{U}}_R Y_{Qu_i} u_{iL} + \bar{\tilde{D}}_R Y_{Qd_i} d_{iL}) + \Phi^\dagger\sum_{i=1}^{3}(\bar{\tilde{U}}_L Y_{Uu_i} u_{iR} + \bar{\tilde{D}}_L Y_{Dd_i} d_{iR}) + \text{H.c.} \tag{4}$$

Here, $\mathrm{SU}(2)_L$ symmetry imposes

$$Y_{Qu_i} = \sum_{j=1}^{3} V^*_{u_i d_j} Y_{Qd_j}, \tag{5}$$

for $i = 1, 2, 3$, where $V_{u_i d_j}$ is an element of the Cabibbo-Kobayashi-Maskawa (CKM) matrix.

Integrating out the heavy vectorlike quarks, one obtains the effective Z' couplings to the SM quarks as

$$\mathcal{L}_{\rm eff} \supset -Z'_\alpha \sum_{i,j=1}^{3} (g^L_{u_i u_j} \bar{u}_{iL} \gamma^\alpha u_{jL} + g^R_{u_i u_j} \bar{u}_{iR} \gamma^\alpha u_{jR} + g^L_{d_i d_j} \bar{d}_{iL} \gamma^\alpha d_{jL} + g^R_{d_i d_j} \bar{d}_{iR} \gamma^\alpha d_{jR}), \tag{6}$$

where

$$g^L_{u_i u_j} = +g' \frac{Y^*_{Qu_i} Y_{Qu_j} v_\Phi^2}{2m_Q^2}, \quad g^R_{u_i u_j} = -g' \frac{Y^*_{Uu_i} Y_{Uu_j} v_\Phi^2}{2m_U^2},$$
$$g^L_{d_i d_j} = +g' \frac{Y^*_{Qd_i} Y_{Qd_j} v_\Phi^2}{2m_Q^2}, \quad g^R_{d_i d_j} = -g' \frac{Y^*_{Dd_i} Y_{Dd_j} v_\Phi^2}{2m_D^2}. \tag{7}$$

The effective couplings to $t \to c$ currents, for instance, are generated by the diagrams shown in Fig. 1.

After integrating out Q, U, and D, the Yukawa mixing couplings in Eq. (4) also induce the effective couplings of Φ to the SM quark bilinears. In particular, the physical mode of the Φ field, ϕ, may couple to the top and charm quarks; hence, the top FCNC decay $t \to c\phi$ can occur if the ϕ boson is lighter than the top. In this paper, we concentrate on the decay $t \to cZ'$, assuming that the ϕ is heavier than the top. The phenomenology of the U(1)′ Higgs boson ϕ will be investigated elsewhere [26].

B. P_5' and R_K anomalies

The effective bsZ' couplings in Eq. (7), in combination with Eq. (2), induce extra contributions to $b \to s\mu^+\mu^-$ decays. Assuming the Z' is heavy compared to the B meson mass scale, one may integrate out the Z' and obtain the BSM contributions to the $b \to s$ effective Hamiltonian,

$$\Delta C_9^\mu (\bar{s}\gamma_\alpha P_L b)(\bar{\mu}\gamma^\alpha \mu) + C_9'^\mu (\bar{s}\gamma_\alpha P_R b)(\bar{\mu}\gamma^\alpha \mu), \tag{8}$$

with the Wilson coefficients

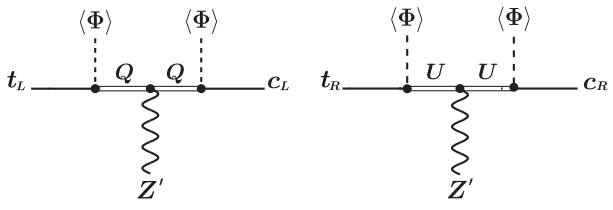

FIG. 1. Diagrams that induce effective tcZ' couplings.

$$\Delta C_9^\mu \simeq +\frac{Y^*_{Qs} Y_{Qb}}{2m_Q^2}, \qquad C_9'^\mu \simeq -\frac{Y^*_{Ds} Y_{Db}}{2m_D^2}, \tag{9}$$

where g' and v_Φ cancel out in the final expressions. Note that the electron counterparts are unchanged, i.e., $\Delta C_9^e = C_9'^e = 0$, resulting in the violation of lepton flavor universality in $b \to s\ell^+\ell^-$ between $\ell = \mu, e$.

In Ref. [15], the values $\Delta C_9^\mu \simeq -(35\ \text{TeV})^{-2}$, $C_9'^\mu \simeq +(35\ \text{TeV})^{-2}$ from a global analysis [6] of $b \to s$ data were adopted as a solution for the P_5' anomaly [2]. Since then, the R_K anomaly [4] has emerged, while P_5' has been updated by LHCb with the 3 fb^{-1} data set [3]. A recent global analysis [14], after the P_5' update, found the best-fit values $\Delta C_9^\mu \simeq -(34\ \text{TeV})^{-2}$, $C_9'^\mu \simeq +(54\ \text{TeV})^{-2}$. We remark that this fit does not include $b \to se^+e^-$ modes, while R_K is defined by the ratio $R_K \equiv \mathcal{B}(B^+ \to K^+\mu^+\mu^-)/\mathcal{B}(B^+ \to K^+e^+e^-)$. The measured R_K value [4] is better explained by $C_9'^\mu \sim 0$ with a ΔC_9^μ value similar to the above best-fit value, which is still within the 1σ ellipse of the allowed region in Ref. [14]. For illustration, therefore, we take the following values as a reference point to solve the $b \to s$ anomalies:

$$\Delta C_9^\mu \simeq -(34\ \text{TeV})^{-2}, \qquad C_9'^\mu \sim 0. \tag{10}$$

Interpreted within the Z' model, the values of Eq. (10) correspond to[2]

$$m_Q \simeq 24\ \text{TeV} \times (-Y_{Qb} Y^*_{Qs})^{1/2}, \tag{11}$$

with real and negative $Y_{Qb}Y^*_{Qs}$, and $Y_{Db}Y^*_{Ds}/m_D^2 \sim 0$. The latter implies the vectorlike quark D is decoupled. For hierarchical Yukawa couplings ($Y_{Qb} = 1$, $Y_{Qs} = -\lambda^2$ with $\lambda \simeq 0.23$), Eq. (11) implies $m_Q \simeq 5.5$ TeV.

C. Constraints on v_Φ

Before entering a discussion on the $t \to cZ'$ decay, we summarize constraints on v_Φ, the VEV of the U(1)′ Higgs field, which is of great importance to $t \to cZ'$.

The most significant constraint comes from neutrino trident production, i.e., $\nu_\mu N \to \nu_\mu N \mu^+\mu^-$, with the normalized cross section [15]

$$\frac{\sigma}{\sigma_{\rm SM}} \simeq \frac{1 + (1 + 4s_W^2 + 2v^2/v_\Phi^2)^2}{1 + (1 + 4s_W^2)^2}, \tag{12}$$

for a heavy Z'. Using CCFR data [27], which imply $\sigma_{\rm exp}/\sigma_{\rm SM} = 0.82 \pm 0.28$, we obtain the 2σ lower bound

$$v_\Phi \gtrsim 540\ \text{GeV} \quad \text{for } m_{Z'} \gtrsim 10\ \text{GeV}. \tag{13}$$

[2]Note that the sign for $Y_{Qb}Y^*_{Qs}$ is opposite to the one in Ref. [15].

For a fixed $m_{Z'}$, this constraint can be translated into an upper bound on $g' = m_{Z'}/v_\Phi$, i.e., $g' \lesssim 0.09\times(m_{Z'}/50\ \text{GeV})$. For $m_{Z'} \lesssim 10$ GeV, the constraint is softened [21], as we will see in the next section.

For a Z' lighter than the Z boson, the coupling g' is also constrained by $Z \to 4\ell$ searches at the LHC. An analysis [15,21] that utilizes the Run 1 result of ATLAS [28] found that $Z \to 4\ell$ provides slightly tighter constraints than the neutrino trident production for 9 GeV $\lesssim m_{Z'} \lesssim$ 50 GeV.[3] The strongest bound, $g' \lesssim 0.01$, is attained for $m_{Z'} \sim 10$ GeV, leading to $v_\Phi \gtrsim 1000$ GeV around this mass value. This loses sensitivity for lower Z' masses due to the cut applied in the experimental analysis.

For $m_{Z'} \gg m_\mu$, the Z' contribution to muon $g-2$ is given by $\Delta a_\mu \simeq m_\mu^2/(12\pi^2 v_\Phi^2)$ [20]. To explain the discrepancy between experiment and theory, $\Delta a_\mu = (2.9 \pm 0.9)\times 10^{-9}$ [19], one needs 160 GeV $\lesssim v_\Phi \lesssim$ 220 GeV. This range is excluded by the constraint from the neutrino trident production, Eq. (13). The case for the light Z' will be discussed in the next section.

The effective bsZ' coupling induces B_s mixing, which provides an upper bound on v_Φ. The modification to the B_s mixing amplitude is given by [15]

$$\frac{M_{12}}{M_{12}^{\rm SM}} \simeq 1 + (Y_{Qb}Y_{Qs}^*)^2\left(\frac{v_\Phi^2}{m_Q^4} + \frac{1}{16\pi^2}\frac{1}{m_Q^2}\right) \times \left[\frac{g_2^4}{16\pi^2}\frac{1}{m_W^2}(V_{ts}^*V_{tb})^2 S_0\right]^{-1}, \quad (14)$$

where $S_0 \simeq 2.3$ and the D quark effects are decoupled, given the $b \to s$ transition data. It is useful to eliminate the dependence on $Y_{Qb}Y_{Qs}^*/m_Q^2$ in terms of ΔC_9^μ of Eq. (9) [30]. Then, allowing BSM effects up to 15% [15], we find the upper bound

$$v_\Phi \lesssim 5.6\ \text{TeV}\left(\frac{(34\ \text{TeV})^{-2}}{|\Delta C_9^\mu|}\right). \quad (15)$$

We have neglected the $1/m_Q^2$ term in Eq. (14), which is numerically valid for $m_Q \lesssim 10$ TeV. For larger m_Q, the bound gets gradually stronger, e.g., $v_\Phi \lesssim 5.4(3.9)$ TeV for $m_Q = 20(50)$ TeV, with ΔC_9^μ satisfying Eq. (10).

The constraint from kaon mixing can be avoided by assuming the mixing of Q and D quarks with d quark is suppressed, $Y_{Qd} \simeq Y_{Dd} \simeq 0$. Although this assumption leads to $Y_{Qu} \simeq \lambda Y_{Qs}$ via Eq. (5) (and is, hence, a new contribution to D mixing), B_s mixing still gives the strongest constraint [15]. We further set $Y_{Uu} \simeq 0$, to switch off the right-handed $c \to u$ current contribution to D mixing, in order to pursue the possibility of a large $t \to cZ'$ rate.

[3]For a recent study of the Z' search in $Z \to 4\ell$, see also [29].

D. Branching ratio for $t \to cZ'$

We now turn to $t \to cZ'$ decay. With the effective tcZ' couplings in Eq. (7), the decay rate is given by

$$\Gamma(t \to cZ') = \frac{m_t}{32\pi}\lambda^{1/2}(1,x_c,x')[(|g_{ct}^L|^2 + |g_{ct}^R|^2)[1 + x_c - 2x' + (1-x_c)^2/x'] - 12\,\text{Re}(g_{ct}^R g_{ct}^{L*})\sqrt{x_c}], \quad (16)$$

where $x_c \equiv m_c^2/m_t^2$, $x' \equiv m_{Z'}^2/m_t^2$ and

$$\lambda(x,y,z) \equiv x^2 + y^2 + z^2 - 2(xy + yz + zx). \quad (17)$$

Taking the ratio with the $t \to bW$ rate, the $t \to cZ'$ branching ratio is given by

$$\mathcal{B}(t \to cZ') \simeq \frac{(1-x')^2(1+2x')}{2(1-x_W)^2(1+2x_W)} \times \left(|Y_{Qt}Y_{Qc}^*|^2\frac{v^2v_\Phi^2}{4m_Q^4} + |Y_{Ut}Y_{Uc}^*|^2\frac{v^2v_\Phi^2}{4m_U^4}\right), \quad (18)$$

where $x_W \equiv m_W^2/m_t^2$, and we have set $m_c^2/m_t^2, m_b^2/m_t^2 \to 0$. Note that our result is a factor of 4 smaller than the one shown in Ref. [15].

The first term in Eq. (18) is induced by the left-handed $t \to c$ current (Fig. 1, left), which is related to the left-handed $b \to s$ current by $\text{SU}(2)_L$ symmetry. Neglecting Cabibbo-suppressed terms, Eq. (5) implies $Y_{Qt} \sim Y_{Qb}$, $Y_{Qc} \sim Y_{Qs}$. One may eliminate the $Y_{Qt}Y_{Qc}^*/m_Q^2$ dependence in Eq. (18) by using ΔC_9^μ [Eq. (9)] to rewrite the left-handed current contribution,

$$\mathcal{B}(t \to cZ')_{\rm LH} \simeq \frac{(1-x')^2(1+2x')}{2(1-x_W)^2(1+2x_W)}|\Delta C_9^\mu|^2 v^2 v_\Phi^2. \quad (19)$$

Applying the lower bound [Eq. (13)] and the upper bound [Eq. (15)] on v_Φ, we obtain the following allowed range for the left-handed current contribution:

$$0.7\times 10^{-8} \lesssim \mathcal{B}(t \to cZ')_{\rm LH} \lesssim 0.8\times 10^{-6}, \quad (20)$$

for a Z' mass sufficiently below the kinematic threshold. Note that the lower limit assumes the central value of ΔC_9^μ from the global fit in Eq. (10), while the upper limit is insensitive to ΔC_9^μ as the dependence cancels out. The branching ratio can be slightly larger than the upper value quoted in Ref. [15], i.e., few $\times 10^{-7}$. This is because the B_s-mixing constraint on v_Φ, Eq. (15), is weakened due to the decoupling of D quark effects, which is favored by the measured R_K value.

On the other hand, the second term in Eq. (18), induced by the right-handed $t \to c$ current (Fig. 1, right), is not related to FCNCs in the down-type quark sector. Treating

m_U, Y_{Ut}, and Y_{Uc} as free parameters, the right-handed current contribution can be easily enhanced over the left-handed current contribution. To see how large it can be, we introduce a mixing parameter between the vectorlike quark U and t_R or c_R as

$$\delta_{Uq} \equiv \frac{Y_{Uq} v_\Phi}{\sqrt{2} m_U}, \qquad (q = t, c) \tag{21}$$

and recast the right-handed current contribution as

$$\mathcal{B}(t \to cZ')_{\rm RH} \simeq \frac{(1-x')^2(1+2x')}{2(1-x_W)^2(1+2x_W)} \frac{v^2}{v_\Phi^2} |\delta_{Ut}\delta_{Uc}^*|^2. \tag{22}$$

For fixed values of δ_{Ut} and δ_{Uc}, this can be enhanced by lowering the value of v_Φ, which is bounded from below by neutrino trident production [Eq. (13)]. Taking reasonably large mixing parameters $\delta_{Ut} = \delta_{Uc} \simeq \lambda$ for illustration, Eq. (13) implies

$$\mathcal{B}(t \to cZ')_{\rm RH} \lesssim 3 \times 10^{-4} \quad (\delta_{Ut} = \delta_{Uc} \simeq \lambda). \tag{23}$$

This is smaller than the value in Ref. [15], i.e., ∼1%, partially because of the correction factor 1/4 in Eq. (18). In the corrected formula, the ∼1% branching ratio requires rather large mixing parameters, $\delta_{Ut} \sim \delta_{Uc} \sim 0.5$.

In Fig. 2, contours of $\mathcal{B}(t \to cZ')_{\rm RH}$ are given in the (Y_{Ut}, Y_{Uc}) plane for $m_{Z'} = 50$ GeV, $g' = 0.064$, $v_\Phi = 780$ GeV, and $m_U = 2.5$ TeV. The vertical (horizontal) dashed lines mark the value of Y_{Ut} (Y_{Uc}) above which the mixing parameter $\delta_{Ut}(\delta_{Uc})$ exceeds λ. These lines are placed as a rough indication for a reasonable range of Yukawa mixing couplings Y_{Uq}. The figure illustrates that $\mathcal{B}(t \to cZ')_{\rm RH}$ can exceed 10^{-4} for $Y_{Ut}, Y_{Uc} \sim 1$, with δ_{Ut}, $\delta_{Uc} < \lambda$ satisfied.

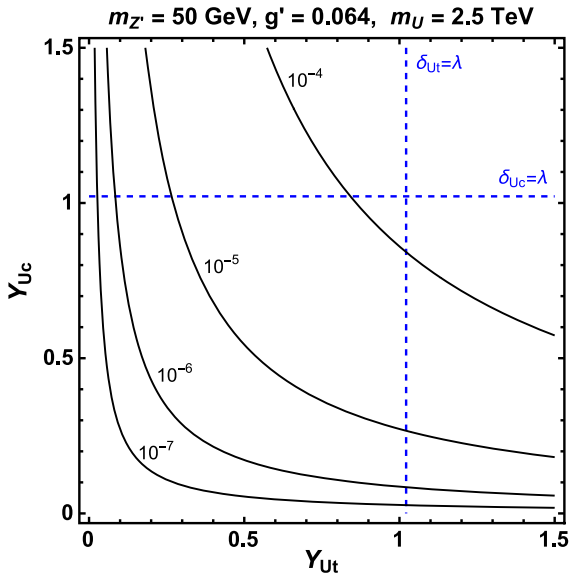

FIG. 2. Contours for $\mathcal{B}(t \to cZ')_{\rm RH}$ in the (Y_{Ut}, Y_{Uc}) plane for $m_{Z'} = 50$ GeV, $g' = 0.064$, $v_\Phi = 780$ GeV, and $m_U = 2.5$ TeV. In estimating $\mathcal{B}(t \to cZ')$, only the contribution from the second term in Eq. (18), i.e., the right-handed $t \to c$ current, is included. The vertical (horizontal) blue dashed line marks the value of Y_{Ut} (Y_{Uc}) above which the mixing parameter $\delta_{Ut}(\delta_{Uc})$ exceeds $\lambda \simeq 0.23$.

Before turning to search at the LHC, we provide the partial widths for Z' decay,

$$\Gamma(Z' \to \ell^+\ell^-) = \frac{g'^2}{12\pi} m_{Z'} \left[1 - \frac{4m_\ell^2}{m_{Z'}^2}\right]^{\frac{1}{2}} \left[1 + \frac{2m_\ell^2}{m_{Z'}^2}\right],$$
$$\Gamma(Z' \to \nu_\ell \bar{\nu}_\ell) = \frac{g'^2}{24\pi} m_{Z'}, \tag{24}$$

where $\ell = \mu, \tau$. The approximate branching ratios are

$$\mathcal{B}_{\tau\tau} \simeq \mathcal{B}_{\mu\mu} \simeq \mathcal{B}_{\nu\nu} \simeq \frac{1}{3} \quad (2m_\tau \ll m_{Z'}),$$
$$\mathcal{B}_{\mu\mu} \simeq \mathcal{B}_{\nu\nu} \simeq \frac{1}{2} \quad (2m_\mu \ll m_{Z'} < 2m_\tau),$$
$$\mathcal{B}_{\nu\nu} = 1 \quad (m_{Z'} < 2m_\mu). \tag{25}$$

E. $t \to cZ'$ search at the LHC

The decay $t \to cZ'$ followed by $Z' \to \ell^+\ell^-$ ($\ell = \mu, \tau$) can be searched for in $t\bar{t}$ events at the LHC. It is similar to $t \to qZ$ ($q = u, c$) decay, which has been searched for by the ATLAS [31] and CMS [32] experiments using $t\bar{t} \to Zq + Wb$ with leptonically decaying Z and W, resulting in a final state with three charged leptons. The $t \to cZ'$ decay with a heavy Z' should be searched for in an analogous way, i.e., by modifying event selection criteria for an opposite-sign-charged lepton pair.

The current best limit on the $t \to qZ$ rate comes from the CMS analysis with the full Run 1 data set [32], finding $\mathcal{B}(t \to qZ) < 5 \times 10^{-4}$ at 95% C.L., while ATLAS [31], based on the 20.3 fb^{-1} data set of the 8 TeV run, found $\mathcal{B}(t \to qZ) < 7 \times 10^{-4}$ at 95% C.L. These limits should be improved with more data during the 13–14 TeV run of the LHC. The expected limits at the 14 TeV LHC with 300 fb^{-1} (3000 fb^{-1}) data are $\mathcal{B}(t \to qZ) < 2.7 \times 10^{-4} (1.0 \times 10^{-4})$ for CMS [33][4] and $\mathcal{B}(t \to qZ) < 2.2 \times 10^{-4}$ (7×10^{-5}) for ATLAS [36,37].

For illustration, we attempt a reinterpretation of the CMS limits for $t \to cZ$ to the case for $t \to cZ'$ by a simple scaling of the Z and Z' decay branching ratios into the charged leptons ($\ell = e, \mu$). An advantage of the $t \to cZ'$ search is

[4]In the Snowmass white paper [34], a more optimistic value of ∼10^{-5} is quoted as the CMS sensitivity for $t \to qZ$ with 300 fb^{-1} data at the 14 TeV LHC. This was based on extrapolating from the 7 TeV result [35]. The projections in Ref. [33], on the other hand, are based on a Monte Carlo analysis.

the larger Z' branching ratio, e.g., $\mathcal{B}(Z' \to \mu^+\mu^-) \simeq 1/3$ for $m_{Z'} \gg 2m_\tau$ compared with $\mathcal{B}(Z \to \ell^+\ell^-) \simeq 0.07$ (summed over e and μ). Multiplying the factor of $\mathcal{B}(Z \to \ell^+\ell^-)/\mathcal{B}(Z' \to \ell^+\ell^-) \simeq 0.2$ to the current [32] and future [33] CMS limits for $t \to cZ$, we infer sensitivities for $t \to cZ'(\to \mu^+\mu^-)$ by CMS as

$$\mathcal{B}(t \to cZ') \lesssim \begin{cases} 10^{-4} & \text{(CMS Run 1)}, \\ 5 \times 10^{-5} & \text{(CMS 300 fb}^{-1}\text{)}, \\ 2 \times 10^{-5} & \text{(CMS 3000 fb}^{-1}\text{)} \end{cases} \quad (26)$$

for a heavy Z' with $m_{Z'} \sim \mathcal{O}(10)$ GeV. The scaling of the ATLAS limits gives similar results. Therefore, the right-handed-current-induced $t \to cZ'$ might already be probed by Run 1 data (see Fig. 2), while the left-handed current contribution seems to be beyond the sensitivity of LHC, even with 3000 fb^{-1} data [see Eq. (20)].

For a light Z' with $2m_\mu < m_{Z'} \lesssim 400$ MeV, the scaling factor is slightly reduced as $\mathcal{B}(Z \to \ell^+\ell^-)/\mathcal{B}(Z' \to \ell^+\ell^-) \simeq 0.14$ due to larger $Z' \to \mu^+\mu^-$ branching ratio ($\simeq 1/2$). For such a light Z', however, the search strategy needs to be changed. In particular, muon pairs produced by boosted Z' bosons would be highly collimated, while the existing $t \to qZ$ search requires events with isolated charged leptons. Nevertheless, we adopt Eq. (26) for the light Z' case as target values in the following analysis.

For a light Z' with $m_{Z'} < 2m_\mu$, the Z' decays only into neutrino pairs. Thus, the search at the LHC would be quite challenging.[5]

III. MUON $g-2$ AND Z'

In this and following sections, we consider the light Z' scenarios motivated by the muon $g-2$ anomaly. In Fig. 3, we give the parameter region (blue band) in the $(m_{Z'}, g')$ plane that accounts for the discrepancy [20], $\Delta a_\mu = (2.9 \pm 0.9) \times 10^{-9}$ [19], taking 2σ error range. The parameter space is strongly constrained [21] by neutrino trident production, the gray-shaded exclusion region. Thus, the Z' boson of $L_\mu - L_\tau$ symmetry can explain the muon $g-2$ anomaly only if $m_{Z'} \lesssim 400$ MeV, as given in Eq. (1). In this section, we consider the $t \to cZ'$ decay in the scenario of

$$2m_\mu < m_{Z'} \lesssim 400 \text{ MeV}, \quad \text{[scenario (iia)]} \quad (27)$$

which permits the $Z' \to \mu^+\mu^-$ decay.

The Z' lifetime, $\tau_{Z'}$, estimated by summing up Eqs. (24), is also given in Fig. 3 as the solid black contours. We see that $\tau_{Z'} \lesssim 0.1$ fs for the muon $g-2$ favored region above the dimuon threshold. The decay length of a light Z' with energy $E_{Z'}$ is given by

$$\gamma c\tau_{Z'} \simeq 0.4\ \mu\text{m} \left[\frac{2}{N_{\text{eff}}}\right] \left[\frac{10^{-3}}{g'}\right]^2 \left[\frac{0.3\text{ GeV}}{m_{Z'}}\right]^2 \left[\frac{E_{Z'}}{10\text{ GeV}}\right], \quad (28)$$

where $N_{\text{eff}} \simeq 2$ for $2m_\mu \ll m_{Z'} < 2m_\tau$ and $N_{\text{eff}} \simeq 1$ for $m_{Z'} < 2m_\mu$. Thus, for $m_{Z'} \gtrsim 2m_\mu$, the Z' that is motivated by muon $(g-2)$ decays promptly after production at colliders such as LHC and B factories, with branching ratios approximately shown in Eq. (25). For $m_{Z'} < 2m_\mu$, the lifetime can be significantly longer for an extremely light Z', but its existence is simply felt as a missing energy (with no missing mass) in collider experiments, regardless of its decay.

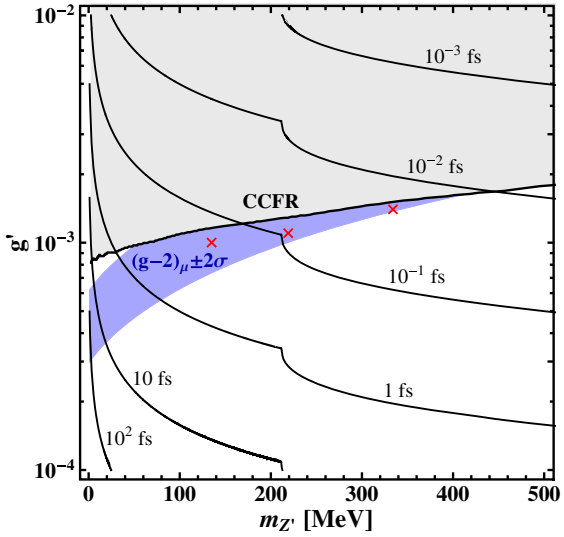

FIG. 3. Lifetime of a light Z' with relevant constraints in the $(m_{Z'}, g')$ plane: solid lines are labeled contours for $\tau_{Z'}$, the blue-shaded band is the region favored by muon $g-2$ within 2σ [19], and the gray-shaded region is excluded by neutrino trident production [27] and taken from Ref. [21]. The red crosses at $(m_{Z'}, g') = (135\text{ MeV}, 10^{-3})$, $(219\text{ MeV}, 1.1 \times 10^{-3})$, $(334\text{ MeV}, 1.4 \times 10^{-3})$ indicate benchmark points adopted in our numerical study, as explained in the text.

A. FCNC B decays

As the Z' mass range in Eq. (27) is too low to explain the P_5' and R_K anomalies, we treat rare B meson decay data as providing constraints on the effective bsZ' coupling. By $\text{SU}(2)_L$ symmetry, this also constrains the left-handed tcZ' coupling. In the light Z' scenario, rare B meson decays provide rather strong constraints, and even the right-handed tcZ' coupling becomes significantly constrained at the one-loop level. We also discuss rare kaon decay constraints on the latter.

[5]The $t \to q$ $(q = u, c)$ decay with missing energy has been discussed based on dark-matter models [38,39].

1. $B \to K^{(*)} Z'$ formulas

The light Z' can be produced directly in $B \to K^{(*)} Z'$ decays, with $Z' \to \mu^+\mu^-/\nu\bar{\nu}$. For the bsZ' couplings of Eq. (6), the branching ratio is given by[6]

$$\mathcal{B}(\bar{B} \to \bar{K} Z') = \frac{|g^L_{sb} + g^R_{sb}|^2}{64\pi} \frac{m_B^3 \beta^3_{BKZ'}}{m^2_{Z'}\Gamma_B} [f_+^{BK}(m^2_{Z'})]^2, \quad (29)$$

where f_+^{BK} is the $B \to K$ form factor and

$$\beta_{XYZ} \equiv \lambda^{1/2}(1, m_Y^2/m_X^2, m_Z^2/m_X^2), \quad (30)$$

with $\lambda(x, y, z)$ defined in Eq. (17). For $B \to K^* Z'$, the branching ratio can be expressed as [40]

$$\mathcal{B}(\bar{B} \to K^* Z') = \frac{\beta_{BK^*Z'}}{16\pi m_B \Gamma_B} (|H_0|^2 + |H_+|^2 + |H_-|^2), \quad (31)$$

where the helicity amplitudes $H_{0,\pm}$ are given by

$$\begin{aligned} H_0 &= (g^L_{sb} - g^R_{sb}) \left[-\frac{1}{2}(m_B + m_{K^*}) \xi A_1(m^2_{Z'}) \right. \\ &\quad \left. + \frac{m_{K^*} m_{Z'}}{m_B + m_{K^*}} (\xi^2 - 1) A_2(m^2_{Z'}) \right], \\ H_\pm &= \frac{1}{2}(g^L_{sb} - g^R_{sb})(m_B + m_{K^*}) A_1(m^2_{Z'}) \\ &\quad \pm (g^L_{sb} + g^R_{sb}) \frac{m_{K^*} m_{Z'}}{m_B + m_{K^*}} \sqrt{\xi^2 - 1} V(m^2_{Z'}), \end{aligned} \quad (32)$$

with $\xi \equiv (m_B^2 - m^2_{K^*} - m^2_{Z'})/(2 m_{K^*} m_{Z'})$, and A_1, A_2, V are $B \to K^*$ form factors. For the form factor numerical values, we adopt the fit formulas from light-cone sum rule calculations [41,42]. As the Z' couples to the muon through the vector current, there is no new physics contribution to $B_s \to \mu^+\mu^-$.

For later convenience, we provide numerical expressions of the $B^+ \to K^+ Z'$ and $B^0 \to K^{*0} Z'$ branching ratios for $m_{Z'} \lesssim 400$ MeV,

$$\begin{aligned} \mathcal{B}(B^+ \to K^+ Z') &\simeq 2.2 \times 10^{12} |g^L_{sb} + g^R_{sb}|^2 \left(\frac{300\ \text{MeV}}{m_{Z'}} \right)^2, \\ \mathcal{B}(B^0 \to K^{*0} Z') &\simeq 2.4 \times 10^{12} |g^L_{sb} - g^R_{sb}|^2 \left(\frac{300\ \text{MeV}}{m_{Z'}} \right)^2 \\ &\quad + 1.4 \times 10^{10} |g^L_{sb} + g^R_{sb}|^2. \end{aligned} \quad (33)$$

Note that the $(m_B/m_{Z'})^2$ enhancement comes from the longitudinally polarized Z'.

[6]We imply both $B^0 \to K^0 Z'$ and $B^\pm \to K^\pm Z'$. A similar convention applies to $B \to K^* Z'$.

2. $B \to K^{(*)} \mu^+\mu^-$ data

With ~50% Z' decaying into muon pairs, $B \to K^{(*)} Z'$ decays would leave footprints in the dimuon mass ($q^2 = m^2_{\mu\mu}$) spectra of $B \to K^{(*)}\mu^+\mu^-$ decays. As the SM prediction is not reliable for $q^2 < 1\ \text{GeV}^2$ [43], one challenge for the search of low-mass new bosons is the estimation of SM background. Instead, one could take a data-based approach [44] by searching for a narrow peak in the dimuon spectrum. With full 3.0 fb^{-1} Run 1 data, the LHCb experiment has performed such a dedicated search for a new hidden-sector boson χ in $B^0 \to K^{*0}\chi$ with $\chi \to \mu^+\mu^-$ [45]. Scanning the dimuon spectrum for 214 MeV $\leq m_{\mu\mu} \leq$ 4350 MeV and finding no evidence for a signal, upper limits of $\mathcal{O}(10^{-9})$ on $\mathcal{B}(B^0 \to K^{*0}\chi)\mathcal{B}(\chi \to \mu^+\mu^-)$ are set for most of the m_χ range with $\tau_\chi \leq 100$ ps.

As the LHCb analysis assumed χ to be scalar [45], the upper limits could be different for the Z' case due to a difference in efficiency. We estimated the ratio of efficiency for vector vs scalar boson, based on information in the Supplemental Material of Ref. [45], and confirmed that the change is rather small, varying within 0%–20% in the mass range of our interest (see Appendix A for detail). Hence, we can apply directly the limits in Ref. [45],

$$\mathcal{B}(B^0 \to K^{*0}\chi)\mathcal{B}(\chi \to \mu\mu) \lesssim (0.8 - 6.3) \times 10^{-9} \quad \text{(LHCb)}, \quad (34)$$

at 95% C.L. for 214 MeV $\leq m_\chi \leq$ 400 MeV, with $\tau_\chi \ll 1$ ps. As the width of the Z' is very small, we neglect the interference between the Z' and the SM contributions.

The LHCb result greatly improves the previous limit set by Belle [46],

$$\mathcal{B}(B^0 \to K^{*0} X)\mathcal{B}(X \to \mu\mu) \lesssim (2.3 - 5.0) \times 10^{-8} \quad \text{(Belle)}, \quad (35)$$

at 90% C.L. for a vector boson X with mass 212 MeV $\leq m_X \leq$ 300 MeV. However, the Belle result complements that of LHCb for the range 212 MeV $\leq m_X \leq$ 214 MeV just above the dimuon threshold of 211.3 MeV.

There are no existing results for the dedicated search of low-mass new bosons in the $B \to K\mu^+\mu^-$ mode. We stress the importance of searching in this mode, as the two decay modes are complementary in probing the chiral structure of bsZ' couplings: the $B \to KZ'$ rate depends on the vector-like combination $g^L_{sb} + g^R_{sb}$, while the $B \to K^* Z'$ rate is sensitive to the axial-vector combination $g^L_{sb} - g^R_{sb}$, as can be read from Eq. (33).

In a previous study [22], published before the advent of the LHCb analysis [45], we attempted at constraining the Z' effect using existing LHCb data for $B^+ \to K^+\mu^+\mu^-$. We chose the 1 fb^{-1} result [47] instead of the 3 fb^{-1} one [48],

as the latter provides the dimuon spectrum only for $q^2 > 0.1\ \mathrm{GeV}^2 \simeq (316\ \mathrm{MeV})^2$, which covers only half the Z' mass range in scenario (iia). The 1 fb^{-1} result, however, gives the spectrum for $q^2 > 0.05\ \mathrm{GeV}^2$, which can probe $m_{Z'}$ down to 224 MeV. In contrast to $B \to K^* \mu^+ \mu^-$, the photon peak is absent in $B^+ \to K^+ \mu^+ \mu^-$, and the measured q^2 spectrum [47] is rather flat in the low-q^2 range, with average differential branching ratio $d\mathcal{B}/dq^2 = (2.41 \pm 0.22) \times 10^{-8}\ \mathrm{GeV}^2$ in $1\ \mathrm{GeV}^2 < q^2 < 6\ \mathrm{GeV}^2$. Treating this as background, we subtracted it from the measured value of $d\mathcal{B}/dq^2 = (2.85 \pm 0.30) \times 10^{-8}\ \mathrm{GeV}^{-2}$ in the lowest q^2 bin of $0.05\ \mathrm{GeV}^2 < q^2 < 2.00\ \mathrm{GeV}^2$. We then estimated the allowed range of the Z' contribution in this bin, $\Delta\mathcal{B}(B^+ \to K^+ \mu^+ \mu^-) = (0.86 \pm 0.59) \times 10^{-8}$. At 2σ, this reads [22]

$$\mathcal{B}(B^+ \to K^+ Z')\mathcal{B}(Z' \to \mu^+ \mu^-) \lesssim 2.0 \times 10^{-8} \quad \text{(LHCb)} \tag{36}$$

for $224\ \mathrm{MeV} \lesssim m_{Z'} \lesssim 1414\ \mathrm{MeV}$.

3. $B \to K^{(*)} \nu\bar{\nu}$ data

In scenario (iia), the other ~50% of Z' bosons decay into neutrino pairs, resulting in $B \to K^{(*)} \nu\bar{\nu}$. Sensitivities of experimental searches for $B \to K^{(*)} \nu\bar{\nu}$ by the *BABAR* [49] and Belle [50] experiments are still above the SM level. For our purpose, the *BABAR* result [49] is useful, as model-independent constraints on BSM effects are given for spectra of $s_B \equiv m_{\nu\nu}^2/m_B^2$ bin by bin. From Fig. 6 of Ref. [49], the first bin $0 < s_B < 0.1$, or $0 < m_{\nu\nu} \lesssim 1670$ MeV, gives the constraints $\Delta\mathcal{B}(B^+ \to K^+ \nu\bar{\nu}) = (0.35^{+0.60}_{-0.15}) \times 10^{-5}$ and $\Delta\mathcal{B}(B^+ \to K^{*+} \nu\bar{\nu}) = (-0.1^{+1.9}_{-0.3}) \times 10^{-5}$. The other two decay modes with K^0 or K^{*0} give weaker limits. The K^+ channel favors nonzero BSM effects due to the observation of a small excess over the expected background. However, the probability to observe such an excess in the signal region is 8.4%; hence, it is not significant. The above limits at 2σ imply, for $0 < m_{Z'} \lesssim 1670$ MeV,

$$0.05 < 10^5 \mathcal{B}(B^+ \to K^+ Z')\mathcal{B}(Z' \to \nu\bar{\nu}) < 1.55,$$
$$10^5 \mathcal{B}(B^+ \to K^{*+} Z')\mathcal{B}(Z' \to \nu\bar{\nu}) < 3.7 \quad (BABAR). \tag{37}$$

Given the Z' branching ratios $\mathcal{B}_{\mu\mu} \sim \mathcal{B}_{\nu\nu} \sim 1/2$, the excess in $B^+ \to K^+ \nu\bar{\nu}$ is not compatible with the LHCb limit on $B^+ \to K^+ Z'(\to \mu^+ \mu^-)$, Eq. (36). In scenario (iia), we therefore treat the *BABAR* limits just as a reference, except when the Z' mass is close to the dimuon threshold and the $B \to K^{(*)} \mu^+ \mu^-$ limits do not apply.

B. $t \to cZ'$ via left-handed current

The $B \to K^* Z'$ rate is sensitive to the combination $g^L_{sb} - g^R_{sb}$, while its dependence on $g^L_{sb} + g^R_{sb}$ is weaker, as can be seen from Eq. (33). Hence, the limits on $B^0 \to K^{*0} Z'(\to \mu^+ \mu^-)$ by LHCb, Eq. (34), draw an ellipse extending along the $g^L_{sb} = g^R_{sb}$ direction on the (g^L_{sb}, g^R_{sb}) plane for each $m_{Z'}$ value. The resulting constraints on the bsZ' couplings are $|g^L_{sb}|, |g^R_{sb}| \lesssim (2-7) \times 10^{-10}$ for $214\ \mathrm{MeV} \le m_{Z'} \le 400\ \mathrm{MeV}$.

The constraints on the bsZ' couplings are improved if the limit on $B^+ \to K^+ Z'(\to \mu^+ \mu^-)$ extracted from the LHCb data, Eq. (36), is further imposed: $|g^L_{sb}|, |g^R_{sb}| \lesssim 1 \times 10^{-10}$ for $224\ \mathrm{MeV} \lesssim m_{Z'} \le 400\ \mathrm{MeV}$, which is rather stable with respect to $m_{Z'}$. The limit implies

$$m_Q \gtrsim 670\ \mathrm{TeV} \sqrt{|Y^*_{Qs} Y_{Qb}| \left(\frac{m_{Z'}}{300\ \mathrm{MeV}}\right) \left(\frac{10^{-3}}{g'}\right)}, \tag{38}$$

which is an order of magnitude larger than in scenario (i) [Eq. (11)]. Assuming the $\mathrm{SU}(2)_L$ relation $g^L_{ct} \simeq g^L_{sb}$, then, we obtain bounds on the left-handed current contribution to the $t \to cZ'$ branching ratio,

$$\mathcal{B}(t \to cZ')_{\mathrm{LH}} \lesssim (3-4) \times 10^{-15}, \tag{39}$$

for $224\ \mathrm{MeV} \lesssim m_{Z'} \le 400\ \mathrm{MeV}$. These values would be too small to measure even with the high-luminosity LHC upgrade. [See Eq. (26) for a naive expectation.]

For $214\ \mathrm{MeV} \le m_{Z'} \lesssim 224\ \mathrm{MeV}$, the $B^+ \to K^+ Z'(\to \mu^+ \mu^-)$ limit does not apply, and bounds on the $t \to cZ'$ rate are weakened,

$$\mathcal{B}(t \to cZ')_{\mathrm{LH}} \lesssim (2-4) \times 10^{-13}, \tag{40}$$

for $214\ \mathrm{MeV} \le m_{Z'} \lesssim 224\ \mathrm{MeV}$. In the narrow interval $212\ \mathrm{MeV} \le m_{Z'} < 214\ \mathrm{MeV}$, the LHCb limits on $B^0 \to K^{*0} Z'(\to \mu^+ \mu^-)$ are taken over by the Belle limits, Eq. (35), which give bounds that are an order of magnitude weaker on $\mathcal{B}(t \to cZ')_{\mathrm{LH}}$ than the case for $214\ \mathrm{MeV} \le m_{Z'} \lesssim 224\ \mathrm{MeV}$. The remaining spot of $211.3\ \mathrm{MeV} \lesssim m_{Z'} < 212\ \mathrm{MeV}$, just above the dimuon threshold, is still constrained by the *BABAR* limits on $B \to K^{(*)} \nu\bar{\nu}$, Eq. (37); this leads to $\mathcal{B}(t \to cZ')_{\mathrm{LH}} \lesssim 4 \times 10^{-12}$, which is further diluted by a small Z' branching ratio $\mathcal{B}(Z' \to \mu^+ \mu^-) \lesssim 10\%$. Note that the excess in $B^+ \to K^+ \nu\bar{\nu}$ does not necessarily imply a nonzero $g^L_{sb} \simeq g^L_{ct}$, as g^R_{sb} alone can still explain the excess. These values of $\mathcal{B}(t \to cZ')_{\mathrm{LH}}$ would be still too small for measurements at the LHC.

In deriving the limits on the left-handed current contribution to $\mathcal{B}(t \to cZ')$, we assumed the $\mathrm{SU}(2)_L$ relation $g^L_{ct} \simeq g^L_{sb}$. This is valid for $Y_{Qt} \sim Y_{Qc}$, but does not hold in general. More precisely, the $\mathrm{SU}(2)_L$ relation is given by

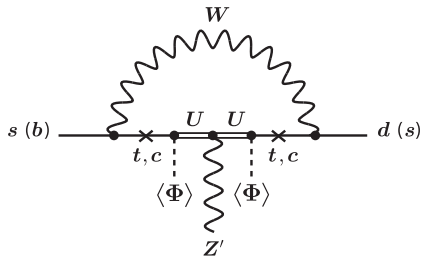

FIG. 4. Feynman diagram that induces the effective sdZ' (bsZ') coupling at one-loop through Yukawa couplings Y_{Ut} and Y_{Uc}. The crosses indicate quark mass insertions which flip chirality for t or c. We included similar contribution from the would-be Nambu-Goldstone bosons.

Eq. (5): $Y_{Qb} = V_{cb}Y_{Qc} + V_{tb}Y_{Qt} \simeq A\lambda^2 Y_{Qc} + Y_{Qt}$ and $Y_{Qs} = V_{cs}Y_{Qc} + V_{ts}Y_{Qt} \simeq Y_{Qc} - A\lambda^2 Y_{Qt}$, where $A \simeq 0.81$ [1] and Y_{Qu} is taken to be zero to avoid D meson constraints. A remarkable deviation from our assumption occurs when $Y_{Qc}/Y_{Qt} \sim \lambda^2$: Y_{Qs} vanishes for $Y_{Qc} \simeq A\lambda^2 Y_{Qt}$; hence, $g^L_{sb} \propto Y^*_{Qs}Y_{Qb} \simeq 0$ (and $g^L_{ds} \simeq 0$). This allows a large g^L_{ct} without violating the $b \to sZ'$ (and $s \to dZ'$) constraints. Yet, this implies $Y_{Qd} \sim \lambda Y_{Qc}$ with $Y_{Qb} \simeq Y_{Qt}$; hence, $g^L_{db} \propto Y^*_{Qd}Y_{Qb} \sim \lambda g^L_{ct}$, which would be constrained by the measurement of the $B^+ \to \pi^+\mu^+\mu^-$ decay by LHCb [51,52], as well as $B - \bar{B}$ mixing. We do not pursue such an extreme case in this paper.

Before moving on, we briefly mention the B_s meson mixing constraint. For a light Z', the local $(\bar{s}b)(\bar{s}b)$ box operator construction in usual renormalization group analysis is not valid, as the Z' remains a dynamical degree of freedom at the m_B scale. Here, we simply recover the momentum dependence in the Z' propagator in the usual heavy Z' formula and set the Z' momentum to the B_s mass scale. To see the impact of this constraint, for simplicity, we only include the left-handed bsZ' coupling effects. Employing the unitarity gauge and the vacuum insertion approximation [7], we find that the $B_s - \bar{B}_s$ mixing amplitude is modified as

$$\frac{M_{12}}{M_{12}^{\rm SM}} \simeq 1 - \frac{(g^L_{sb})^2 v^2}{m^2_{B_s} - m^2_{Z'}}\left(1 - \frac{5}{8}\frac{m^2_{B_s}}{m^2_{Z'}}\right) \times \left[\frac{g_2^2}{16\pi^2}(V^*_{ts}V_{tb})^2 S_0\right]^{-1}. \quad (41)$$

Allowing a 15% BSM effect, we obtain $|g^L_{sb}| \lesssim 2\times 10^{-6}(m_{Z'}/300\ \text{MeV})$, four orders of magnitude weaker than the constraint from $B \to K^{(*)}Z'(\to \mu^+\mu^-)$.

[7]For a more careful treatment of light vector boson effects on B_s mixing, see, e.g., [40].

C. Right-handed tcZ' coupling: Loop-induced down-quark sector FCNCs

The right-handed tcZ' coupling induces FCNCs in the down-type quark sector at the one-loop level. More precisely, the $\mathrm{SU}(2)_L$ singlet vectorlike quark U, responsible for the effective right-handed tcZ' coupling, mediates the diagram in Fig. 4, leading to extra contributions to effective sdZ' and bsZ' couplings. Assisted by the SM charged current couplings of the W boson to left-handed quarks, the flavor-diagonal ttZ' and the ccZ' contribute in addition to the tcZ'. These contributions are loop, chirality, and CKM suppressed. There are thus no significant impacts for a heavy Z'. However, for a light Z', the loop-induced FCNC decays give meaningful constraints, as the meson decay rates are hugely enhanced due to the on-shell nature of the Z', compensating these suppressions.

In estimating the loop-induced FCNC couplings, for simplicity we set $Y_{Qd_i} = Y_{Dd_i} = 0$ ($i = 1, 2, 3$) to turn off the tree-level FCNC couplings in the down-type quark sector. We further set $Y_{Uu} = 0$ to avoid constraints from D meson decays and mixing, for the sake of maximizing the $t \to cZ'$ decay rate. We are then left with the Yukawa mixing couplings for the vectorlike quark U to right-handed top or charm quarks, Y_{Ut} and Y_{Uc}.

Working in the 't Hooft-Feynman gauge, we calculate the diagram of Fig. 4 as well as similar contributions with the would-be Nambu-Goldstone bosons. We neglect the external momenta as usual, but keep all internal momenta, including the one for the vectorlike quark U. We then obtain the loop-induced effective couplings [22],

$$\mathcal{L}_{\rm eff} \supset \Delta g^L_{d_i d_j}\bar{d}_{iL}\gamma^\alpha d_{jL}Z'_\alpha + \text{H.c.}, \quad (42)$$

where $i, j = 1, 2, 3$, and

$$\Delta g^L_{d_i d_j} = \frac{g' v_\Phi^2}{32\pi^2 v^2}[V_{td_j}V^*_{td_i}\kappa_{tt}f_{tt} + (V_{td_j}V^*_{cd_i}\kappa_{tc} + V_{cd_j}V^*_{td_i}\kappa_{ct})f_{ct} + V_{cd_j}V^*_{cd_i}\kappa_{cc}f_{cc}], \quad (43)$$

with

$$\kappa_{u_k u_l} = Y_{Uu_k}Y^*_{Uu_l}\frac{m_{u_k}m_{u_l}}{m_U^2}, \quad (44)$$

and

$$f_{tt} \simeq \frac{3m_W^2}{m_t^2 - m_W^2}\left(1 - \frac{m_W^2}{m_t^2 - m_W^2}\log\frac{m_t^2}{m_W^2}\right) + \log\frac{m_U^2}{m_t^2},$$
$$f_{ct} \simeq 1 + \log\frac{m_U^2}{m_t^2} + \frac{3m_W^2}{m_t^2 - m_W^2}\log\frac{m_t^2}{m_W^2},$$
$$f_{cc} \simeq 4\log\frac{m_W^2}{m_c^2} + \log\frac{m_U^2}{m_W^2} - 3. \quad (45)$$

The expressions for these loop functions are in the large-m_U limit. Exact expressions used in our numerical study are given in Appendix B.

In the loop-induced bsZ' and bdZ' couplings, Eq. (43), the top-top loop contribution dominates due to the chiral factor, provided that Y_{Uc}/Y_{Ut} is not too large. Then, $\Delta g^L_{db}/\Delta g^L_{sb} \simeq V^*_{td}/V^*_{ts} \sim \lambda$; hence, the ratio $\mathcal{B}(b \to dZ')/\mathcal{B}(b \to sZ') \sim \lambda^2 \simeq 0.05$ is SM-like. For large Y_{Uc} (e.g., $Y_{Uc}/Y_{Ut} \gtrsim 4$ for $m_U = 2$ TeV), the top-charm loop contribution becomes dominant. Even in this case, $\Delta g^L_{db}/\Delta g^L_{sb} \simeq V^*_{cd}/V^*_{cs} \sim \lambda$; hence, the ratio $\mathcal{B}(b \to dZ')/\mathcal{B}(b \to sZ')$ is still SM-like. Thus, the better-measured $b \to s$ decays are more suitable to watch the Z' effect than $b \to d$. We consider $b \to sZ'$ and $s \to dZ'$ decays below.

D. FCNC K decays

1. $K \to \pi Z'$ formulas

One can obtain $\mathcal{B}(B \to K^{(*)}Z')$ for loop-induced bsZ' coupling by replacing $g^L_{sb} \to \Delta g^L_{sb}$, $g^R_{sb} \to 0$ in Eqs. (29) and (31). Then, $\mathcal{B}(B \to K^*Z') \simeq \mathcal{B}(B \to KZ')$, as can be seen from Eq. (33). Hence, the LHCb limits on $B^0 \to K^{*0}\chi(\to \mu^+\mu^-)$, Eq. (34), give the strongest constraint in most $m_{Z'}$ ranges of scenario (iia).

The loop-induced sdZ' coupling causes $K \to \pi Z'$ for $m_{Z'} < m_K - m_\pi$, leading to $K \to \pi\mu^+\mu^-$ and $K \to \pi\nu\bar{\nu}$ decays. The branching ratios for $K^+ \to \pi^+Z'$ and $K_L \to \pi^0 Z'$ decays are given by

$$\mathcal{B}(K^+ \to \pi^+ Z') = \frac{|\Delta g^L_{ds}|^2}{64\pi}\frac{m^3_{K^+}}{m^2_{Z'}\Gamma_{K^+}}\beta^3_{K^+\pi^+Z'}[f_+^{K^+\pi^+}(m^2_{Z'})]^2,$$
$$\mathcal{B}(K_L \to \pi^0 Z') = \frac{[\mathrm{Im}(\Delta g^L_{ds})]^2}{64\pi}\frac{m^3_{K_L}}{m^2_{Z'}\Gamma_{K_L}}\beta^3_{K_L\pi^0Z'}[f_+^{K^0\pi^0}(m^2_{Z'})]^2, \quad (46)$$

where $\beta_{K\pi Z'}$ is defined by Eq. (30), and $f_+^{K\pi}$ are the $K \to \pi$ form factors. For the latter, we adopt the result of Ref. [53], which is based on the partial next-to-next-to-leading order calculation with isospin-breaking effects in chiral perturbation theory. In estimating the $K_L \to \pi^0 Z'$ rate, we took $|K_L\rangle \simeq (|K^0\rangle + |\bar{K}^0\rangle)/\sqrt{2}$ with the phase convention where $CP|K^0\rangle = -|\bar{K}^0\rangle$, neglecting CP violation in kaon mixing. The branching ratio for $K_S \to \pi^0 Z'$ can be obtained from the one for $K_L \to \pi^0 Z'$ with the replacements $\mathrm{Im}(\Delta g^L_{ds}) \to \mathrm{Re}(\Delta g^L_{ds})$ and $\tau_{K_L} \to \tau_{K_S}$.

2. $K \to \pi\mu^+\mu^-$ data

In the SM, the $K^+ \to \pi^+\mu^+\mu^-$ decay is dominated by long-distance effects via one-photon exchange $K^+ \to \pi^+\gamma^*$. The decay can be described by chiral perturbation theory [54] with the dimuon invariant mass spectrum $d\Gamma/dz \propto |W(z)|^2$, where $z \equiv m^2_{\mu\mu}/m^2_{K^+}$ and $W(z)$ is the $K \to \pi\gamma^*$ form factor. The most precise value for $\mathcal{B}(K^+ \to \pi^+\mu^+\mu^-)$ by a single measurement comes from the NA48/2 experiment [55] at the CERN SPS. The measured z spectrum in the whole kinematic range of $4m^2_\mu/m^2_{K^+} \le z \le (1 - m_{\pi^+}/m_{K^+})^2$, corresponding to 211 MeV $\lesssim m_{\mu\mu} \lesssim$ 354 MeV, is reasonably described by various form factor models. In particular, the measured z spectrum does not exhibit significant excesses over the fit curve by the linear form factor model. Here, we attempt a simple data-based approach to extract reasonable sizes for possible Z' effects.

In a previous study [22], we focused on the largest upward deviation from the fit curve in the z spectrum of NA48/2, which is located in the $z \in (0.32, 0.34)$ bin, corresponding to $m_{\mu\mu} \in (279, 288)$ MeV. Subtracting the fit value from the measured one, we read the allowed range for an extra contribution, $\Delta(d\Gamma/dz) \simeq (2.5 \pm 1.5) \times 10^{-24}$ GeV. This corresponds to the deviation of the branching ratio in $m_{\mu\mu} \in (279, 288)$ MeV, $\Delta\mathcal{B}(K^+ \to \pi^+\mu^+\mu^-) \simeq (9.4 \pm 5.6) \times 10^{-10}$. Allowing a 2σ range, we estimate the limit on the Z' contribution, $\mathcal{B}(K^+ \to \pi^+Z')\mathcal{B}(Z' \to \mu^+\mu^-) \lesssim 2.1 \times 10^{-9}$ for 279 MeV $\lesssim m_{Z'} \lesssim$ 288 MeV. The constraint is tighter for other Z' mass values in 211 MeV $\lesssim m_{\mu\mu} \lesssim$ 354 MeV. For instance, we obtain

$$\mathcal{B}(K^+ \to \pi^+Z')\mathcal{B}(Z' \to \mu\mu) \lesssim 1.1 \times 10^{-9} \quad \text{(NA48/2)} \quad (47)$$

for 327 MeV $< m_{Z'} \lesssim$ 335 MeV, and

$$\mathcal{B}(K^+ \to \pi^+Z')\mathcal{B}(Z' \to \mu\mu) \lesssim 1.2 \times 10^{-9} \quad \text{(NA48/2)} \quad (48)$$

for $2m_\mu < m_{Z'} \lesssim$ 221 MeV.

For $K_L \to \pi^0\mu^+\mu^-$, the current best limit comes from KTeV [56] at Fermilab, giving the 90% C.L. limit

$$\mathcal{B}(K_L \to \pi^0\mu^+\mu^-) < 3.8 \times 10^{-10} \quad \text{(KTeV)}. \quad (49)$$

This is above the SM prediction of $(1.29^{+0.24}_{-0.23}) \times 10^{-11}$ [57]. We thus impose the above limit on $\mathcal{B}(K_L \to \pi^0 Z')\mathcal{B}(Z' \to \mu^+\mu^-)$ for $2m_\mu < m_{Z'} <$ 350 MeV, covered by the kinematic selection of the KTeV analysis.

The $K_S \to \pi^0\mu^+\mu^-$ mode was measured by NA48/1 [58] at CERN SPS, giving $\mathcal{B}(K_S \to \pi^0\mu^+\mu^-) = [2.9^{+1.5}_{-1.2}(\mathrm{stat}) \pm 0.2(\mathrm{syst})] \times 10^{-9}$. This was used as input in the SM prediction of $K_L \to \pi^0\mu^+\mu^-$ [57] to control the indirect CP-violating contribution. For the possible Z' contribution, isospin symmetry implies $\mathcal{B}(K_S \to \pi^0 Z') \lesssim (\tau_{K_S}/\tau_{K^+})\mathcal{B}(K^+ \to \pi^0 Z') \simeq 0.007 \times \mathcal{B}(K^+ \to \pi^0 Z')$. Given that the experimental sensitivity on the $K^+ \to \pi^+Z'(\to \mu^+\mu^-)$ branching ratio is around 10^{-9}, the above isospin relation constrains the $K_S \to \pi^0 Z'(\to \mu^+\mu^-)$ branching

ratio to be within $\sim 10^{-11}$, which may be beyond the sensitivity of NA48/1 data.

3. $K \to \pi\nu\bar{\nu}$ data

For $K^+ \to \pi^+\nu\bar{\nu}$ decay, the E949 experiment at BNL [59], together with its predecessor E787, reported $\mathcal{B}(K^+ \to \pi^+\nu\bar{\nu}) = (1.73^{+1.15}_{-1.05}) \times 10^{-10}$, which is consistent with the SM prediction of $(8.25 \pm 0.64) \times 10^{-11}$ [57]. The measurement error is large and E787/E949 [60] also reported the 90% C.L. upper limit of $\mathcal{B}(K^+ \to \pi^+\nu\bar{\nu}) < 3.35 \times 10^{-10}$. We remark, however, that the experimental analyses utilized limited intervals for the pion momentum p_{π^+}, or equivalently the neutrino pair mass $m_{\nu\nu}$, to avoid blinding backgrounds from $K^+ \to \pi^+\pi^0$ and $K^+ \to \pi^+\pi^-\pi^+/\pi^+\pi^0\pi^0$: one is the $\pi\nu\bar{\nu}(1)$ region, where 211 MeV $< p_{\pi^+} <$ 229 MeV, or $0 \le m_{\nu\nu} \lesssim 116$ MeV; the other is the $\pi\nu\bar{\nu}(2)$ region, where 140 MeV $< p_{\pi^+} <$ 199 MeV, or 152 MeV $\lesssim m_{\nu\nu} \lesssim 261$ MeV. The kinematic selection of the $K^+ \to \pi^+\nu\bar{\nu}$ experiments has an interesting implication for $K_L \to \pi^0\nu\bar{\nu}$ search [22], as we will discuss in the next section.

The E787/E949 data have been used also for a dedicated search [60] of a two-body decay $K^+ \to \pi^+ P^0$ with $P^0 \to \nu\bar{\nu}$, where P^0 is a hypothetical short-lived particle. The upper limits on $\mathcal{B}(K^+ \to \pi^+ P^0)\mathcal{B}(P^0 \to \nu\bar{\nu})$ were given for the mass ranges of $0 \le m_{P^0} \lesssim 125$ MeV or 150 MeV $\lesssim m_{P^0} \lesssim 260$ MeV, which correspond to $\pi\nu\bar{\nu}(1)$ or $\pi\nu\bar{\nu}(2)$ regions, respectively. In the mass range relevant to scenario (iia), the 90% C.L. upper limit increases almost monotonically with mass within

$$\mathcal{B}(K^+ \to \pi^+ P^0)\mathcal{B}(P^0 \to \nu\bar{\nu}) \lesssim (0.4 - 5) \times 10^{-9} \quad \text{(E949)} \tag{50}$$

for $2m_\mu < m_{P^0} \lesssim 260$ MeV.

To facilitate the discussion in scenario (iib), we also quote 90% C.L. upper limits for typical P^0 masses below the dimuon threshold by setting $\mathcal{B}(P^0 \to \nu\bar{\nu}) = 1$. For $0 \le m_{P^0} \lesssim 125$ MeV, the strongest (weakest) bound is attained for $m_{P^0} \simeq 95$ (125) MeV with $\mathcal{B}(K^+ \to \pi^+ P^0) \lesssim 5 \times 10^{-11}(4 \times 10^{-9})$. The bound is rather stable for $0 \le m_{P^0} \lesssim 40$ MeV with $\mathcal{B}(K^+ \to \pi^+ P^0) \lesssim 10^{-10}$. For 150 MeV $\lesssim m_{P^0} < 2m_\mu$, the strongest (weakest) bound is attained for $m_{P^0} \simeq 190$ (150) MeV with $\mathcal{B}(K^+ \to \pi^+ P^0) \lesssim 4 \times 10^{-10}(10^{-8})$.

For the pocket 125 MeV $\lesssim m_{Z'} \lesssim 150$ MeV around the π^0 mass, the upper limit can be still obtained by using the $\pi^0 \to \nu\bar{\nu}$ search in $K^+ \to \pi^+\pi^0$ by E949 [61], $\mathcal{B}(\pi^0 \to \nu\bar{\nu}) < 2.7 \times 10^{-7}$ at 90% C.L. In this search, charged pions with momentum in 198 MeV $< p_{\pi^+} <$ 212 MeV were selected, corresponding to 112 MeV $\lesssim m_{\nu\nu} \lesssim 155$ MeV; hence, the π^0 pocket can be fully covered. Combining this with $\mathcal{B}(K^+ \to \pi^+\pi^0) \simeq 20.7\%$ [1], one has

$$\mathcal{B}(K^+ \to \pi^+ Z') < 5.6 \times 10^{-8} \quad \text{(E949)} \tag{51}$$

at 90% C.L. for $112 \lesssim m_{Z'} \lesssim 155$ MeV.

The $K_L \to \pi^0\nu\bar{\nu}$ decay has been searched for by the E391a experiment [62] at the KEK proton synchrotron, setting the 90% C.L. upper limit

$$\mathcal{B}(K_L \to \pi^0\nu\bar{\nu}) < 2.6 \times 10^{-8} \quad \text{(E391}a\text{)}, \tag{52}$$

without any particular cut on $m_{\nu\nu}$. This is far above the SM prediction of $(2.60 \pm 0.37) \times 10^{-11}$ [57]. Therefore, we impose Eq. (52) on $\mathcal{B}(K_L \to \pi^0 Z')\mathcal{B}(Z' \to \nu\bar{\nu})$ for $m_{Z'} < m_{K_L} - m_{\pi^0} \simeq 363$ MeV. Note that in scenario (iia), where $m_{Z'} > 2m_\mu$, the KTeV limit, Eq. (49), gives a stronger constraint in general, as $\mathcal{B}_{\mu\mu} \sim \mathcal{B}_{\nu\nu} \sim 1/2$. There are no existing constraints on $K_S \to \pi^0\nu\bar{\nu}$, where the branching ratio is suppressed by $\tau_{K_S}/\tau_{K_L} \ll 1$ compared to $K_L \to \pi^0\nu\bar{\nu}$.

E. $t \to cZ'$ via right-handed current

We can now combine all B and K decay data to constrain the right-handed current contribution $\mathcal{B}(t \to cZ')_{\rm RH}$. For illustration, we take the two benchmark points (shown by red crosses in Fig. 3)

(1) $m_{Z'} = 334$ MeV, $g' = 1.4 \times 10^{-3}$, $m_U = 2$ TeV,
(2) $m_{Z'} = 219$ MeV, $g' = 1.1 \times 10^{-3}$, $m_U = 2$ TeV.

The Z' mass values are chosen such that the LHCb limit for $B^0 \to K^{*0}\chi(\to \mu^+\mu^-)$, Eq. (34), is weakened to be tolerant for a possible large $t \to cZ'$ rate: $m_{Z'} = 219$ MeV is one of the points which give the weakest limit in the whole range of 214 MeV $\le m_{Z'} \le 400$ MeV, while $m_{Z'} = 334$ MeV gives the weakest limit in the high mass region 260 MeV $\lesssim m_{Z'} \le 400$ MeV, where the E949 limits for $K^+ \to \pi^+ P^0(\to \nu\bar{\nu})$ do not apply. The two benchmark points are phenomenological representatives of B and K decay constraints. The 95% C.L. upper limits by LHCb [45] are

$$\mathcal{B}(B^0 \to K^{*0}\chi)\mathcal{B}(\chi \to \mu^+\mu^-) < \begin{cases} 4.41 \times 10^{-9} & (m_\chi = 334 \text{ MeV}), \\ 6.29 \times 10^{-9} & (m_\chi = 219 \text{ MeV}). \end{cases} \tag{53}$$

We again neglect the changes in efficiencies from the scalar boson case. For loop-induced bsZ' coupling, where $g^R_{sb} = 0$, the changes are indeed extremely small, up to 6% in the mass range of our interest (see Appendix A). The B and K constraints are summarized in Table I.

In Fig. 5 (left), we give contours of $\mathcal{B}(t \to cZ')_{\rm RH}$ as solid black lines in the (Y_{Ut}, Y_{Uc}) plane for the $m_{Z'} =$ 334 MeV benchmark point. The meson decay constraints are imposed by taking into account the Z' branching ratios, $\mathcal{B}_{\mu\mu} \simeq 48\%$, $\mathcal{B}_{\nu\nu} \simeq 52\%$. The pink-shaded region is allowed by the LHCb bound on $B^0 \to K^{*0}\chi(\to \mu^+\mu^-)$ in Eq. (53). The light-green-shaded regions are favored by the

TABLE I. Summary of B and K decay constraints for the three benchmark points in scenarios (iia) and (iib): $m_{Z'} = 334$, 219, 135 MeV. The numbers shown in third, fourth, and fifth columns are the allowed ranges for each branching ratios, used in Figs. 5–8. See text, and in particular the referred equations (rightmost column), for detail.

Mode	Experiment	$m_{Z'} = 334$ MeV	$m_{Z'} = 219$ MeV	$m_{Z'} = 135$ MeV	Comment
$B^0 \to K^{*0} Z'(\to \mu^+\mu^-)$	LHCb [45]	$< 4.41 \times 10^{-9}$	$< 6.29 \times 10^{-9}$	⋯	See Eq. (53)
$B^+ \to K^+ Z'(\to \nu\bar{\nu})$	*BABAR* [49]	$(0.05, 1.55) \times 10^{-5}$	$(0.05, 1.55) \times 10^{-5}$	$(0.05, 1.55) \times 10^{-5}$	See Eq. (37)
$K^+ \to \pi^+ Z'(\to \mu^+\mu^-)$	NA48/2 [55]	$\lesssim 1.1 \times 10^{-9}$	$\lesssim 1.2 \times 10^{-9}$	⋯	See Eqs. (47), (48)
$K_L \to \pi^0 Z'(\to \mu^+\mu^-)$	KTeV [56]	$< 3.8 \times 10^{-10}$	$< 3.8 \times 10^{-10}$	⋯	See Eq. (49)
$K^+ \to \pi^+ Z'(\to \nu\bar{\nu})$	E787/E949 [60,61]	⋯	$\lesssim 5 \times 10^{-10}$	$< 5.6 \times 10^{-8}$	See Eqs. (50), (51)
$K_L \to \pi^0 Z'(\to \nu\bar{\nu})$	E391a [62]	$< 2.6 \times 10^{-8}$	$< 2.6 \times 10^{-8}$	$< 2.6 \times 10^{-8}$	See Eq. (52)

mild excess in *BABAR* data for $B^+ \to K^+ \nu\bar{\nu}$ at 2σ [Eq. (37)]. The semitransparent dark-gray-shaded region represents the 2σ exclusion by the NA48/2 data for $K^+ \to \pi^+\mu^+\mu^-$, Eq. (47), from our illustration of the limit on the Z' effect. The purple-solid lines are the 90% C.L. exclusion by KTeV data for $K_L \to \pi^0\mu^+\mu^-$, Eq. (49).

All the data have better sensitivity for Y_{Ut} than Y_{Uc}, as the top-top loop contribution dominates the loop-induced effective couplings, Eq. (43), due to m_t/m_c chiral enhancement. The LHCb limit for $B^0 \to K^{*0}\chi(\to \mu^+\mu^-)$ provides the strongest constraint, excluding the *BABAR* region that could account for the $B^+ \to K^+\nu\bar{\nu}$ excess. Nevertheless, the LHCb limit accommodates $\mathcal{B}(t \to cZ')_{\rm RH} \gtrsim 10^{-6}$ along the funnel regions, extending towards large Y_{Uc}. However, the NA48/2 limit for $K^+ \to \pi^+\mu^+\mu^-$ eventually cuts down these funnels. We obtain $\mathcal{B}(t \to cZ')_{\rm RH} \lesssim 2 \times 10^{-5}$.

We remark that $m_{Z'} = 334$ MeV is close to the kinematical limit $m_{K^+} - m_{\pi^+} \simeq 354$ MeV of $K^+ \to \pi^+ Z'$, and the NA48/2 data is less constraining than generic cases. This can be seen from the velocity factor in Eq. (46): $\beta_{K^+\pi^+Z'} \simeq 0.26$ for $m_{Z'} = 334$ MeV, leading to the suppression of $\mathcal{B}(K^+ \to \pi^+ Z')$ by $\beta^3_{K^+\pi^+Z'} \simeq 0.018$, compared with, e.g., $\beta^3_{K^+\pi^+Z'} \simeq 0.31(0.080)$ for $m_{Z'} = 219(300)$ MeV.

For $m_{Z'} > m_{K^+} - m_{\pi^+}$, the two-body decay $K^+ \to \pi^+ Z'$ is kinematically forbidden, and the NA48/2 data loses constraining power; hence, $\mathcal{B}(t \to cZ')_{\rm RH}$ can be arbitrary large along the funnels. However, the funnels imply some degree of fine-tuning between Y_{Ut} and Y_{Uc} with canceled

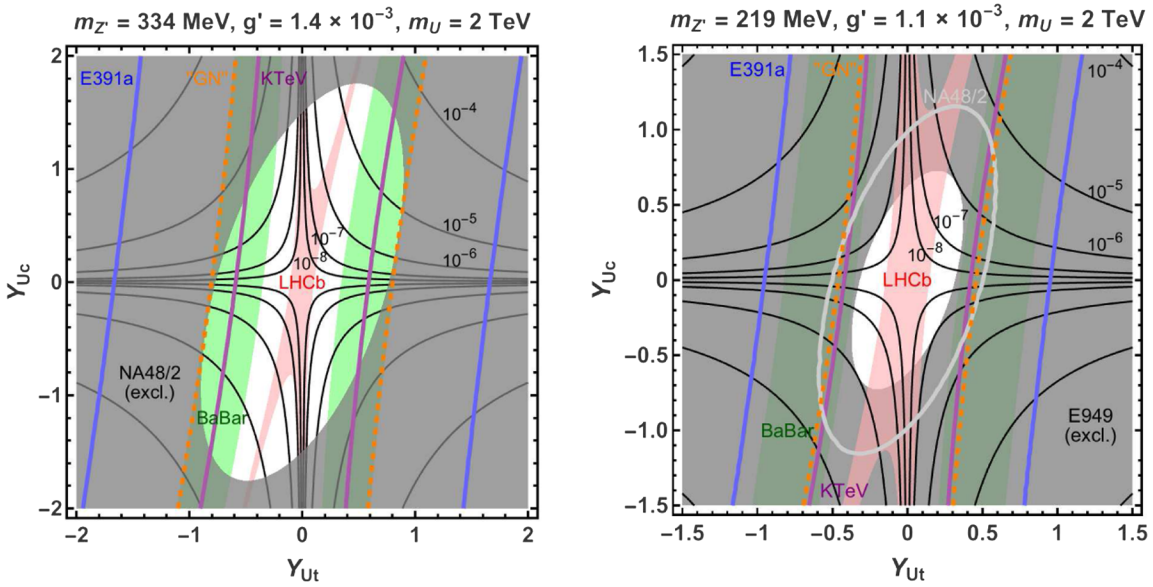

FIG. 5. (Left) Contours of $\mathcal{B}(t \to cZ')_{\rm RH}$ are given as solid black lines in the (Y_{Ut}, Y_{Uc}) plane for $m_{Z'} = 334$ MeV, $g' = 1.4 \times 10^{-3}$, and $m_U = 2$ TeV. The pink-shaded region is allowed by the LHCb 95% C.L. limit for $B^0 \to K^{*0}\chi(\to \mu^+\mu^-)$ in Eq. (53). The light-green-shaded regions are favored by the mild excess in *BABAR* data for $B^+ \to K^+\nu\bar{\nu}$ at 2σ [Eq. (37)]. The semitransparent dark-gray-shaded region represents the 2σ exclusion by NA48/2 for $K^+ \to \pi^+\mu^+\mu^-$, Eq. (47). The solid purple lines are the 90% C.L. exclusion by KTeV for $K_L \to \pi^0\mu^+\mu^-$, Eq. (49). The solid blue lines are the 90% C.L. exclusion by E391a for $K_L \to \pi^0\nu\bar{\nu}$, Eq. (52). The dashed orange lines are the usual GN bound of Eq. (60), explained later. (Right) Same as the left panel, but for $m_{Z'} = 219$ MeV, $g' = 1.1 \times 10^{-3}$, and $m_U = 2$ TeV. Here, the NA48/2 exclusion, Eq. (48), is shown by the light-gray solid line, while the semitransparent dark-gray-shaded region is excluded by the E949 90% C.L. limit $\mathcal{B}(K^+ \to \pi^+ P^0)\mathcal{B}(P^0 \to \nu\bar{\nu}) \lesssim 5 \times 10^{-10}$.

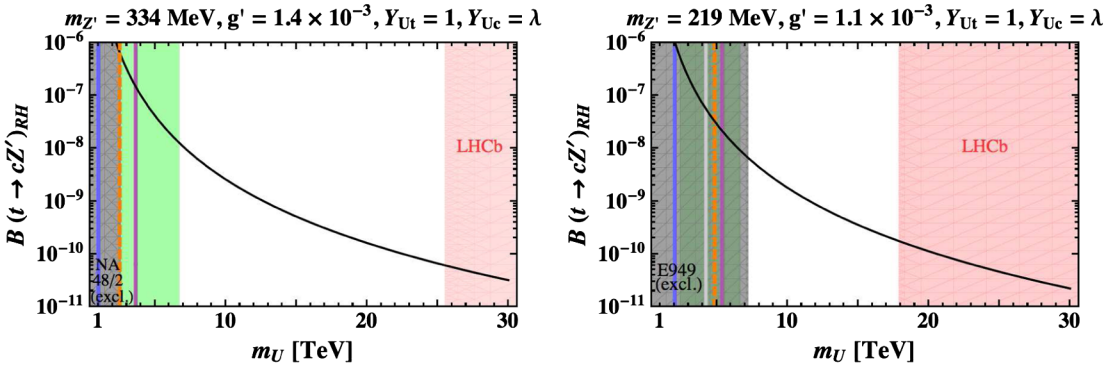

FIG. 6. (Left) Branching ratio $\mathcal{B}(t \to cZ')_{\rm RH}$ of the right-handed-current mediated $t \to cZ'$ as a function of vectorlike quark mass m_U for $m_{Z'} = 334$ MeV and $g' = 1.4 \times 10^{-3}$ with hierarchical Yukawa couplings $Y_{Ut} = 1$, $Y_{Uc} = \lambda \simeq 0.23$. Shaded regions and lines are constraints on m_U from B and K decay data, with the shadings and lines as explained in Fig. 5. (Right) Same as the left panel, but for $m_{Z'} = 219$ MeV and $g' = 1.1 \times 10^{-3}$.

contributions to $b \to sZ'$. Furthermore, to maintain perturbativity, Y_{Uc} should not be too large.

A similar plot for the $m_{Z'} = 219$ MeV benchmark point is given in Fig. 5 (right), where $\mathcal{B}_{\mu\mu} \simeq 28\%$, $\mathcal{B}_{\nu\nu} \simeq 72\%$. In this case, the E949 limit for $K^+ \to \pi^+ P^0 (\to \nu\bar{\nu})$ enters: $\mathcal{B}(K^+ \to \pi^+ P^0)\mathcal{B}(P^0 \to \nu\bar{\nu}) \lesssim 5 \times 10^{-10}$ at 90% C.L. [60], shown as a semitransparent dark-gray-shaded exclusion region. This surpasses the NA48/2 limit for $K^+ \to \pi^+\mu^+\mu^-$, Eq. (48), shown by the light-gray solid ellipse in the figure. The E949 limit fully excludes the funnel regions, and we obtain $\mathcal{B}(t \to cZ')_{\rm RH} \lesssim 0.8 \times 10^{-6}$.

The E949 limit gets stronger towards $m_{Z'} = 2m_\mu$ and generically excludes the funnel regions for $2m_\mu < m_{Z'} \lesssim 230$ MeV, leading to $\mathcal{B}(t \to cZ')_{\rm RH} \lesssim 10^{-6}$. Remarkably, this limit on $\mathcal{B}(t \to cZ')_{\rm RH}$ holds even in the pocket 211.3 MeV $\lesssim m_{Z'} < 212$ MeV, where neither the LHCb nor the Belle limits for $B^0 \to K^{*0} Z' (\to \mu^+\mu^-)$ apply.

We have used $m_U = 2$ TeV, but we obtained similar results for other m_U values. This is because both g^R_{ct} and $\Delta g^L_{sb(ds)}$ are proportional to m_U^{-2}, up to logarithmic dependence, multiplied by a quadratic form in Y_{Ut} and Y_{Uc} [see Eqs. (7) and (43)]. Thus, changing m_U simply results in rescaled Y_{Ut} and Y_{Uc} values. A similar argument applies to the dependence on the U(1)′ coupling g'.

As we took $Y_{Uu} = 0$ to avoid D meson constraints, one might think that $Y_{Ut} > Y_{Uc} > Y_{Uu}$ is the natural ordering of these Yukawa couplings. Taking $Y_{Ut} = 1$ and $Y_{Uc} = \lambda$, we plot $\mathcal{B}(t \to cZ')_{\rm RH}$ in Fig. 6 (left) as a function of m_U for $m_{Z'} = 334$ MeV, with B and K constraints overlaid. In this case, the LHCb constraint is severe, implying $\mathcal{B}(t \to cZ')_{\rm RH} \lesssim 0.6 \times 10^{-10}$. A similar plot for $m_{Z'} = 219$ MeV is given in Fig. 6 (right), where the LHCb limit implies $\mathcal{B}(t \to cZ')_{\rm RH} \lesssim 2 \times 10^{-10}$. The pocket 211.3 MeV $\lesssim m_{Z'} < 212$ MeV is still constrained by E949, giving $\mathcal{B}(t \to cZ')_{\rm RH} \lesssim 3 \times 10^{-9}$.

In short, for the hierarchical Yukawa couplings $Y_{Ut} = 1$, $Y_{Uc} = \lambda$, we obtain $\mathcal{B}(t \to cZ')_{\rm RH} \lesssim \mathcal{O}(10^{-9})$ in the whole mass range of scenario (iia), namely, $2m_\mu < m_{Z'} \lesssim 400$ MeV. These values seem beyond reach of the LHC. On the other hand, if Y_{Ut} and Y_{Uc} are treated as free parameters, $\mathcal{B}(t \to cZ')_{\rm RH}$ can be much larger. In particular, $\mathcal{B}(t \to cZ')_{\rm RH} \sim \mathcal{O}(10^{-5})$ is possible in the funnel regions for appropriately high Z' masses such that the E949 limit is weakened. This may be within reach at the future LHC, as shown in Eq. (26), but a fine-tuned correlation between Y_{Ut} and Y_{Uc} would be needed. Note that our projection for LHC sensitivities is rather naive. A careful collider study should be done to judge the actual sensitivity for $t \to cZ'$ at the LHC.

Surveying other $m_{Z'}$ cases, we find the constraints on $\mathcal{B}(t \to cZ')_{\rm RH}$ in scenario (iia) can be classified into the following three categories:

(1) 330 MeV $\lesssim m_{Z'} \lesssim$ 400 MeV: $\mathcal{B}(t \to cZ')_{\rm RH} \gtrsim 10^{-6}$ is possible along the funnel regions allowed by a hidden-sector boson search of LHCb in $B^0 \to K^{*0}\chi (\to \mu^+\mu^-)$. In particular, if $m_{Z'} \gtrsim m_{K^+} - m_{\pi^+} \simeq 354$ MeV, the K^+ decay constraints can be avoided, and $\mathcal{B}(t \to cZ')_{\rm RH}$ may be arbitrary large for large Y_{Uc}, up to perturbativity and associated fine-tuning of Y_{Ut}.

(2) 230 MeV $\lesssim m_{Z'} \lesssim$ 330 MeV: $\mathcal{B}(t \to cZ')_{\rm RH} \gtrsim 10^{-6}$ is possible along the funnel regions, but $K^+ \to \pi^+\mu^+\mu^-$ (NA48/2) and/or $K^+ \to \pi^+ P^0 (\to \nu\bar{\nu})$ (E949) constraints cut in, such that $\mathcal{B}(t \to cZ')_{\rm RH} \lesssim 10^{-5}$.

(3) $2m_\mu < m_{Z'} \lesssim 230$ MeV: The E949 limit gets stronger towards $m_{Z'} = 2m_\mu$, fully excluding the funnel regions, giving $\mathcal{B}(t \to cZ')_{\rm RH} \lesssim 10^{-6}$ even in the 211.3 MeV $\lesssim m_{Z'} < 212$ MeV pocket, where neither the LHCb nor the Belle limits for $B^0 \to K^{*0} Z' (\to \mu^+\mu^-)$ apply.

We have ignored the interference of the Z' effect with SM contribution, as the Z' width is tiny. We remark, however, that for $m_{Z'} > 2m_\pi$, an absorptive part of $K^+ \to \pi^+\gamma^* (\to \mu^+\mu^-)$ induced by the $\pi\pi$ loop may invalidate the

simple separation of the SM and Z' contributions to $K^+ \to \pi^+\mu^+\mu^-$. This might affect the second mass range, in particular the position where the funnels are cut down by the NA48/2 limit.

IV. A LIGHT Z' THAT EVADES THE GROSSMAN-NIR BOUND

In this section, we study the scenario where

$$m_{Z'} < 2m_\mu \quad \text{[scenario (iib)]}. \tag{54}$$

In this case, the Z' bosons decay exclusively into neutrino pairs and are felt only as missing energy in collider experiments. As such, it would be more challenging to search for $t \to cZ'$ at the LHC. Nevertheless, we estimate for completeness the ranges allowed in this scenario for $t \to cZ'$ branching ratios via left- or right-handed current. The relevant formulas and meson decay constraints were summarized in the previous section.

An interesting outcome of this scrutiny is the possibility, which we previously pointed out [22], that an invisible Z' boson could evade the commonly accepted GN bound [23] of $\mathcal{B}(K_L \to \pi^0\nu\bar{\nu}) \lesssim 1.4 \times 10^{-9}$.

A. $t \to cZ'(\to \nu\bar{\nu})$ via left-handed current

We use *BABAR* data on $B \to K^{(*)}\nu\bar{\nu}$ in Eq. (37) to constrain the tree-level effective bsZ' couplings g^L_{sb} and g^R_{sb}. The 2σ range for $B^+ \to K^+\nu\bar{\nu}$ imposes

$$0.16 \times 10^{-9} \lesssim |g^L_{sb} + g^R_{sb}| \left(\frac{100\ \text{MeV}}{m_{Z'}}\right) \lesssim 0.88 \times 10^{-9}, \tag{55}$$

while the $B^+ \to K^{*+}\nu\bar{\nu}$ data mainly constrains the other combination of the bsZ' couplings,

$$|g^L_{sb} - g^R_{sb}| \left(\frac{100\ \text{MeV}}{m_{Z'}}\right) \lesssim 1.3 \times 10^{-9}. \tag{56}$$

Combining the two constraints, we get

$$|g^L_{sb}|, \qquad |g^R_{sb}| \lesssim 1.1 \times 10^{-9} \left(\frac{m_{Z'}}{100\ \text{MeV}}\right) \tag{57}$$

for $m_{Z'} < 2m_\mu$. Note that the excess in the $B^+ \to K^+\nu\bar{\nu}$ data does not necessarily imply a nonzero g^L_{sb}, as $g^L_{sb} = 0$ can still explain the excess by a nonzero g^R_{sb}.

Using the $SU(2)_L$ relation $g^L_{ct} \simeq g^L_{sb}$, we obtain the upper limit on the left-handed current contribution to the $t \to cZ'$ branching ratio,

$$\mathcal{B}(t \to cZ')_{\text{LH}} \lesssim 4 \times 10^{-12}, \tag{58}$$

for $m_{Z'} < 2m_\mu$. Note that the limit does not depend on $m_{Z'}$, as it cancels out in the final expression.

B. $t \to cZ'(\to \nu\bar{\nu})$ via right-handed current

We constrain the right-handed current contribution to the $t \to cZ'$ branching ratio by using data from $B^+ \to K^+\nu\bar{\nu}$ and $K \to \pi\nu\bar{\nu}$. As discussed in the previous section, the E949 constraint from the $K^+ \to \pi^+P^0(\to \nu\bar{\nu})$ search can be avoided if the Z' mass falls into the π^0-mass window, i.e., 125 MeV $\lesssim m_{Z'} \lesssim$ 150 MeV. Although this mass window is still constrained by $\pi^0 \to \nu\bar{\nu}$, searched in $K^+ \to \pi^+\pi^0$ [Eq. (51)], the limit is rather weak compared to the $K^+ \to \pi^+P^0(\to \nu\bar{\nu})$ limits outside the π^0 window. [See explanation following Eq. (50).] To allow for the possibility of a large $t \to cZ'$ rate, we take the benchmark point $m_{Z'} = 135$ MeV, $g' = 10^{-3}$, $m_U = 2$ TeV, which is shown by a red cross in Fig. 3. The B and K decay constraints are summarized in Table I. As discussed in the previous section, this particular choice of g' and m_U does not affect the final result for $\mathcal{B}(t \to cZ')_{\text{RH}}$.

In Fig. 7, we give contours of $\mathcal{B}(t \to cZ')_{\text{RH}}$ as solid black lines in the (Y_{Ut}, Y_{Uc}) plane. The B and K decay constraints are overlaid with the shadings and line styles as in Fig. 5 (right). The semitransparent dark-gray-shaded region is excluded by the E949 limit on $\pi^0 \to \nu\bar{\nu}$ at 90% C.L. [Eq. (51)]. In the present case, the E391a constraint on $K_L \to \pi^0\nu\bar{\nu}$ [Eq. (52)], shown as solid blue lines, also plays a role. The green-shaded regions, favored by the mild $B^+ \to K^+\nu\bar{\nu}$ excess in *BABAR* data [in Eq. (37)], are compatible with other constraints in most parts of the range shown. This is in contrast to scenario (iia), where the constraints from $B^0 \to K^{*0}\chi(\to \mu^+\mu^-)$ and $K^+ \to \pi^+P^0(\to \nu\bar{\nu})$ exclude the *BABAR* regions. In this benchmark point, we obtain $\mathcal{B}(t \to cZ')_{\text{RH}} \lesssim 5 \times 10^{-5}$.

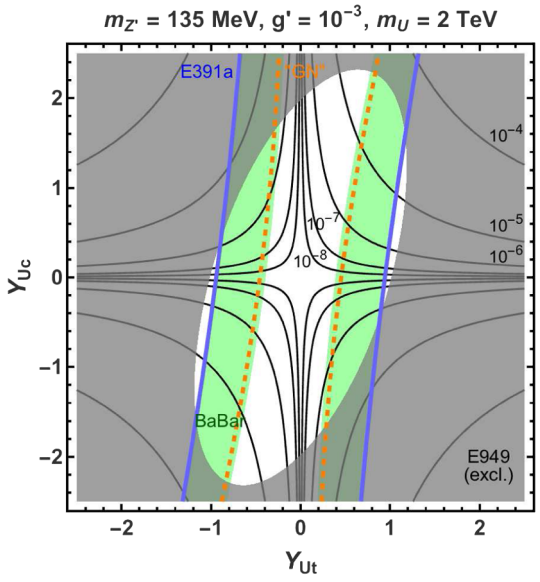

FIG. 7. Same as Fig. 5 (right), but for $m_{Z'} = 135$ MeV and $g' = 10^{-3}$, with the E949 exclusion of Eq. (51).

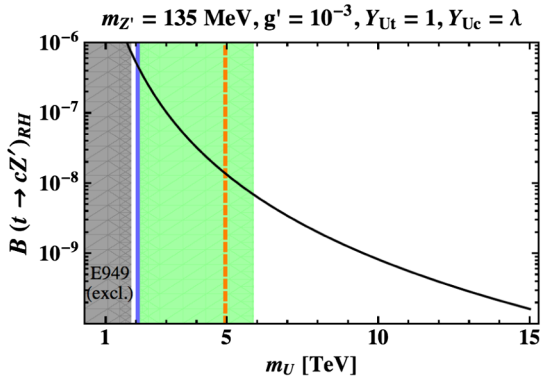

FIG. 8. Same as Fig. 6 (right), but for $m_{Z'} = 135$ MeV and $g' = 10^{-3}$.

Fixing the Yukawa couplings to $Y_{Ut} = 1$, $Y_{Uc} = \lambda$, we plot $\mathcal{B}(t \to cZ')_{\rm RH}$ in Fig. 8 as a function of m_U with the same $m_{Z'}$ and g' values. For this case, the *BABAR* excess favors a nonzero but small $t \to cZ'$ rate within $6 \times 10^{-9} \lesssim \mathcal{B}(t \to cZ')_{\rm RH} \lesssim 5 \times 10^{-7}$.

For the Z' mass within the π^0 window, i.e., 125 MeV $\lesssim m_{Z'} \lesssim$ 150 MeV, the same E949 limit for $K^+ \to \pi^+ Z'$ applies, and we obtain similar results for $\mathcal{B}(t \to cZ')_{\rm RH}$.

The E949 limit gets stronger considerably if the Z' mass is out of the π^0 window; hence, $\mathcal{B}(t \to cZ')_{\rm RH}$ cannot be larger than the above limits. For instance, taking $m_{Z'} =$ 11 MeV with $g' = 5 \times 10^{-4}$, motivated by IceCube data [24,63], we obtain $\mathcal{B}(t \to cZ')_{\rm RH} \lesssim 6 \times 10^{-8}$.

In summary, we obtain $\mathcal{B}(t \to cZ')_{\rm RH} \lesssim 5 \times 10^{-5}$ for any $m_{Z'}$ in scenario (iib). The decay $t \to cZ'(\to \nu\bar{\nu}$ at 100%) with such a small branching ratio might be quite challenging for searches at the LHC.

C. Apparent violation of the Grossman-Nir bound

The light Z' has an interesting implication for kaon decay experiments [22].

From isospin symmetry, the branching ratio $\mathcal{B}(K_L \to \pi^0\nu\bar{\nu})$ is connected with $\mathcal{B}(K^+ \to \pi^+\nu\bar{\nu})$ by a model-independent relation, known as the GN bound [23],

$$\mathcal{B}(K_L \to \pi^0\nu\bar{\nu}) \lesssim 4.3 \times \mathcal{B}(K^+ \to \pi^+\nu\bar{\nu}), \qquad (59)$$

where the overall factor of 4.3 comes from $\tau_{K_L}/\tau_{K^+} \simeq 4.1$ and isospin-breaking effects. Plugging in the 90% C.L. upper limit of $\mathcal{B}(K^+ \to \pi^+\nu\bar{\nu}) < 3.35 \times 10^{-10}$ by E949 [60], the GN bound leads to

$$\mathcal{B}(K_L \to \pi^0\nu\bar{\nu}) \lesssim 1.4 \times 10^{-9} \quad \text{(GN)}. \qquad (60)$$

This is an order of magnitude stronger than the direct limit on $K_L \to \pi^0\nu\bar{\nu}$ by E391a, Eq. (52). In Figs. 5–8, this commonly accepted GN bound is shown by the orange dashed lines.

There are two ongoing experiments in the search for $K \to \pi\nu\bar{\nu}$ decays. The NA62 experiment [64] at CERN aims at measuring of order 100 $K^+ \to \pi^+\nu\bar{\nu}$ events, while the KOTO experiment [65] at J-PARC aims at 3σ measurement of $K_L \to \pi^0\nu\bar{\nu}$ at the SM rate. KOTO has already reached the sensitivity of E391a [Eq. (52)] [66], but folklore is that KOTO can start to probe new physics effects only after Eq. (60) is breached.

We have argued, however, that the kinematic selection in $K^+ \to \pi^+\nu\bar{\nu}$ searches (including both E949 and NA62) makes them insensitive to the possible existence of a light new boson X^0, produced in $K^+ \to \pi^+ X^0$, if $m_{X^0} \sim m_\pi$ or m_{X^0} is larger than $2m_\pi$. If so, the usual GN bound of Eq. (60) does not apply; therefore, without such a selection, KOTO is already entering the domain of new physics.

A relation similar to Eq. (59) still holds for the light Z' contribution, with a slight modification in the overall coefficient. Taking the ratio of the $K_L \to \pi^0 Z'$ and $K^+ \to \pi^+ Z'$ branching ratios in Eq. (46), we obtain the light Z' version of the GN bound,

$$\frac{\mathcal{B}(K_L \to \pi^0 Z')}{\mathcal{B}(K^+ \to \pi^+ Z')} = \frac{\tau_{K_L}}{\tau_{K^+}} \frac{1}{r(m_{Z'}^2)} \left| \frac{\mathrm{Im}(g_{ds}^L + g_{ds}^R)}{g_{ds}^L + g_{ds}^R} \right|^2 \le \frac{\tau_{K_L}}{\tau_{K^+}} \frac{1}{r(m_{Z'}^2)}, \qquad (61)$$

where the isospin breaking factor $r(m_{Z'}^2)$ is defined by

$$\frac{1}{r(m_{Z'}^2)} \equiv \frac{m_{K_L}^3}{m_{K^+}^3} \frac{\beta_{K_L\pi^0Z'}^3}{\beta_{K^+\pi^+Z'}^3} \left[\frac{f_+^{K^0\pi^0}(m_{Z'}^2)}{f_+^{K^+\pi^+}(m_{Z'}^2)} \right]^2. \qquad (62)$$

To keep generality, we recover the dependence on g_{ds}^R, assuming the interaction form of Eq. (6). The form factor ratio is known to be q^2 independent at next-to-leading order in chiral perturbation theory, with numerical value $f_+^{K^+\pi^+}(q^2)/f_+^{K^0\pi^0}(q^2) = 1.0238 \pm 0.0022$ [53]. The genuine GN bound of Eq. (61) is then given by

$$\frac{\mathcal{B}(K_L \to \pi^0 Z')}{\mathcal{B}(K^+ \to \pi^+ Z')} \lesssim 4.122 \left(\frac{1.003}{r(m_{Z'}^2)} \right), \qquad (63)$$

where $r(0) = 1.003$ is taken as reference. The right-hand side, the "GN coefficient," depends on the Z' mass, as illustrated in Fig. 9.

For 125 MeV $\lesssim m_{Z'} \lesssim$ 150 MeV, plugging in the 90% C.L. upper limit on $\mathcal{B}(K^+ \to \pi^+ Z')$ by E949 [Eq. (51)], we obtain $\mathcal{B}(K_L \to \pi^0 Z') \lesssim 2.3 \times 10^{-7}$. The direct bound on $K_L \to \pi^0\nu\bar{\nu}$ by E391a, Eq. (52), is indeed stronger than this true GN bound.

The above argument is general and applicable to any weakly interacting light boson, or short-lived invisibly decaying boson, that couples to $s \to d$ currents. The bound of Eq. (61) holds for a massive vector boson that couples to

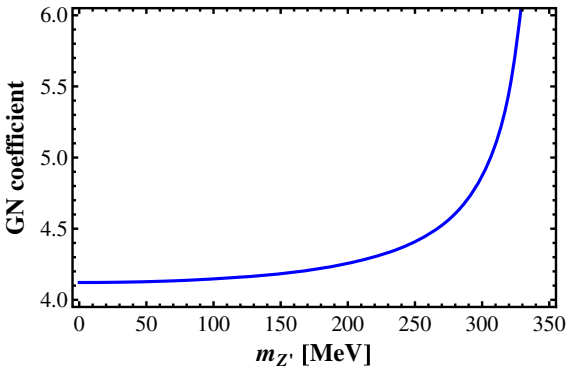

FIG. 9. Maximally allowed value as a function of $m_{Z'}$ for the ratio $\mathcal{B}(K_L \to \pi^0 Z')/\mathcal{B}(K^+ \to \pi^+ Z')$, given in Eq. (61).

the $s \to d$ currents in the form of Eq. (6). On the other hand, for the $L_\mu - L_\tau$ gauge boson with loop-induced sdZ' coupling of Eq. (43), we obtain $|\mathrm{Im}(\Delta g^L_{ds})/g^L_{ds}|^2 \sim |\mathrm{Im}(V_{ts}V^*_{td})/(V_{ts}V^*_{td})|^2 \simeq 0.15$, as long as $Y_{Ut} \gtrsim Y_{Uc}$, due to top-top dominance in the loop. Thus, the GN bound of Eq. (61) cannot be saturated in this case.

The argument can be further extended to three-body kaon decays where the final state contains a pair of new massive invisible particles (χ), i.e., $K \to \pi\chi\chi$. If the mass of χ is larger than m_π, the decay is allowed only if the invariant mass of the χ pair satisfies $2m_\pi < m_{\chi\chi} (< m_K - m_\pi)$. In this case, the π^+ momentum is always outside the signal regions of the $K^+ \to \pi^+ \nu\bar{\nu}$ experiments; hence, the usual GN bound does not apply. An interesting candidate is the very light neutralino in the minimal supersymmetric standard model; this was discussed in Ref. [67], although the analysis needs to be updated in light of recent LHC results. (See Ref. [68] for recent assessment of the light neutralino.)

V. DISCUSSION AND CONCLUSIONS

The so-called P_5' and R_K anomalies in $b \to s$ transitions, as revealed by LHCb data, suggest the possible existence of a new massive gauge boson Z' coupling to the left-handed $b \to s$ current, which in turn implies a tcZ' coupling. Motivated by this, we studied the top FCNC decay $t \to cZ'$ based on the gauged $L_\mu - L_\tau$ model with vectorlike quarks that mix with SM quarks. The model can also be applied to address the muon $g-2$ anomaly, which turns out to allow only a very light Z' due to neutrino scattering data. The situation is mutually exclusive with the $b \to s$ anomalies. We studied how large the $t \to cZ'$ rate can be in three well-motivated scenarios: (i) a heavy Z' with $m_b \lesssim m_{Z'} < m_t - m_c$, motivated by the $P_5{}'$ and R_K anomalies, (iia) a light Z' with $2m_\mu < m_{Z'} \lesssim 400$ MeV, motivated by the muon $g-2$ anomaly, and (iib) the $(g-2)_\mu$-motivated Z' with $m_{Z'} < 2m_\mu$.

In scenario (i), using a global fit result of $b \to s$ data as well as a B_s meson mixing constraint, we find that the left-handed current contribution to branching ratio $\mathcal{B}(t \to cZ')_{\mathrm{LH}}$ can be as large as 10^{-6}. We also find that the right-handed current contribution $\mathcal{B}(t \to cZ')_{\mathrm{RH}}$, which is not constrained by B data, can be as large as $\mathcal{O}(10^{-4})$ with reasonably large mixing (around the Cabibbo angle) between the vectorlike quark U and t, c. The left-handed case would be beyond the reach of even the high-luminosity LHC upgrade, while the right-handed case might be accessible with LHC Run 1 data. [See Eq. (26) for our naive projection based on $t \to qZ$ results.]

In scenario (iia), we find $\mathcal{B}(t \to cZ')_{\mathrm{LH}}$ to be extremely tiny, below 10^{-11}, due to rare B decay constraints. In this scenario, even the right-handed current contribution is constrained by rare B and K decays via one-loop effects. We find that $\mathcal{B}(t \to cZ')_{\mathrm{RH}} \gtrsim 10^{-6}$ is allowed only at the cost of fine-tuning the relation between Y_{Ut} and Y_{Uc}. Nevertheless, in such cancelation regions, $\mathcal{B}(t \to cZ')_{\mathrm{RH}}$ may be larger than $\mathcal{O}(10^{-5})$ for 330 MeV $\lesssim m_{Z'} \lesssim 400$ MeV. Our naive projection based on $t \to qZ$ results suggests that this could be within reach of the ATLAS and CMS experiments with 300^{-1} data at the (13-) 14 TeV LHC. However, a careful collider study is needed to find the true sensitivity, as the search strategy needs to be changed from the $t \to qZ$ case.

Scenario (iib) can accommodate larger $t \to cZ'$ branching ratios for the right-handed current contribution, $\mathcal{B}(t \to cZ')_{\mathrm{RH}} \lesssim 5 \times 10^{-5}$. This case, however, would be more challenging for a collider search, as the Z' decays exclusively into neutrinos (but with little missing mass). Such a light Z' is interesting instead for rare kaon decay experiments, and could even lead to observation of new physics beyond the so-called Grossman-Nir bound, or $\mathcal{B}(K_L \to \pi^0 + \text{nothing}) > 1.4 \times 10^{-9}$. If this happens, our prediction is that it occurs via $K_L \to \pi^0 X^0$ with unobserved $m_{X^0} \sim m_{\pi^0}$, with our Z' motivated by muon $g-2$ as a candidate. We remark that the Z' in scenarios (iia) and (iib) may also be probed by the future neutrino beam facility LBNE [69] via neutrino trident production [21]. In addition, LHCb and Belle II experiments should certainly pursue further "bump" searches in $B \to K^{(*)}\mu^+\mu^-$ and $B \to K^{(*)}\nu\bar{\nu}$ decays.

In this paper, we assumed a particular Z' model to study $t \to cZ'$ decay. In the model, the right-handed tcZ' coupling correlates with the ttZ' and ccZ'couplings. In particular, the ttZ' coupling is strongly constrained by loop-induced decays from chiral m_t/m_c enhancement, and the tcZ' coupling in turn is also constrained indirectly. This correlation is not general, and the meson decay constraints might be relaxed in some other Z' models where the right-handed tcZ' coupling is independent from the ttZ' coupling.

The muon $g-2$ anomaly implies that the U(1)$'$ symmetry breaking scale v_Φ is around the electroweak scale of 246 GeV or below. The mass of the new Higgs boson ϕ

behind the spontaneous breaking of the U(1)′ symmetry is, hence, expected to be below 1 TeV and within reach at the LHC. The mixing of the vectorlike U quark with the top quark via the ϕ-Yukawa interaction leads to effective $tt\phi$ coupling. Thus, the ϕ can be produced via gluon fusion $gg \to \phi$, followed by $\phi \to Z'Z'(\to 4\mu/2\mu 2\nu)$, as pointed out in Ref. [22]. The effective $tt\phi$ coupling, however, is highly suppressed compared to the SM top Yukawa coupling, due to the constraints from $B^0 \to K^{*0}Z'(\to \mu^+\mu^-)$ as discussed in Sec. II; hence, the $gg \to \phi$ cross section is too small to be observed at the LHC [26]. Instead, the effective $tc\phi$ couplings, generated in a similar way as the tcZ', may offer another ϕ production mechanism, i.e., $t \to c\phi$ in $t\bar{t}$ events at the LHC. This gives rise to a striking signature, namely, two collimated dimuons in $pp \to t\bar{t} \to bWc\phi(\to Z'Z')$ with $Z'Z' \to (\mu^+\mu^-)(\mu^+\mu^-)$. This interesting possibility will be pursued elsewhere [26].

ACKNOWLEDGMENTS

K. F. is supported by Research Fellowships of the Japan Society for the Promotion of Science for Young Scientists, Grant No. 15J01079. W. S. H. is supported by Academic Summit Grant No. MOST 103-2745-M-002-001-ASP of the Ministry of Science and Technology, as well as by Grant No. NTU-EPR-103R8915. M. K. is supported under NSC Grant No. 102-2112-M-033-007-MY3. M. K. thanks Y. Chao, A. Mauri, J. Tandean, and M. Williams for valuable discussions. W. S. H. thanks T. Blake and M. Pepe-Altarelli for correspondence. K. F. acknowledges useful correspondence with S. Gori, and thanks the NTUHEP group for hospitality during exchange visits. We thank M. Williams for providing us with the precise upper limits of the hidden-sector boson search by LHCb [45].

APPENDIX A: EFFICIENCY FOR $B^0 \to K^{*0}Z' \to K\pi\mu^+\mu^-$

In order to estimate the efficiency for the $B^0 \to K^{*0}Z' \to K\pi\mu^+\mu^-$ decay at the LHCb, we need information regarding the angular distribution for this decay. In the narrow-width approximation, the normalized differential decay width for $\bar{B}^0 \to \bar{K}^{*0}Z' \to K^-\pi^+\mu^+\mu^-$ is given by

$$\begin{aligned}\frac{1}{\Gamma}\frac{d\Gamma}{d\cos\theta_K d\cos\theta_\ell d\phi} &= \frac{9}{16\pi(1+2m_\mu^2/m_{Z'}^2)(|H_0|^2+|H_+|^2+|H_-|^2)} \\ &\times \{-\beta_\mu^2[|H_0|^2\cos^2\theta_K\cos^2\theta_\ell \\ &+ \frac{1}{4}(|H_+|^2+|H_-|^2)\sin^2\theta_K\sin^2\theta_\ell + \Xi(\theta_K,\theta_\ell,\phi)] \\ &+ |H_0|^2\cos^2\theta_K + \frac{1}{2}(|H_+|^2+|H_-|^2)\sin^2\theta_K\}, \quad \text{(A1)}\end{aligned}$$

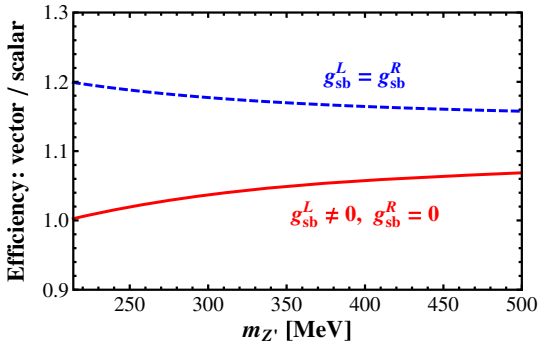

FIG. 10. Ratio of efficiencies between vector-boson Z' and scalar-boson χ for $\bar{B}^0 \to \bar{K}^{*0}Z'(\chi) \to K^-\pi^+\mu^+\mu^-$ events collected by LHCb. The solid line is for $g^L_{sb} \neq 0$, $g^R_{sb} = 0$ and the dashed line is for $g^L_{sb} = g^R_{sb}$. The other two cases of $g^L_{sb} = 0$, $g^R_{sb} \neq 0$ and $g^L_{sb} = -g^R_{sb}$ behave similarly to the solid line.

where $\beta_\mu \equiv \sqrt{1-4m_\mu^2/m_{Z'}^2}$ and the helicity amplitudes $H_{0,\pm}$ are given in Eq. (32). The ϕ dependence enters solely through the function

$$\begin{aligned}\Xi(\theta_K,\theta_\ell,\phi) &= -\frac{1}{4}\sin 2\theta_K \sin 2\theta_\ell\{\cos\phi[\mathrm{Re}(H_0H_+^*)+\mathrm{Re}(H_0H_-^*)] \\ &- \sin\phi[\mathrm{Im}(H_0H_+^*)-\mathrm{Im}(H_0H_-^*)]\} + \frac{1}{2}\sin^2\theta_K\sin^2\theta_\ell \\ &\times [\cos 2\phi\,\mathrm{Re}(H_+H_-^*)+\sin 2\phi\,\mathrm{Im}(H_+H_-^*)]. \quad \text{(A2)}\end{aligned}$$

We follow the LHCb convention [70] for the definition of decay angles: θ_ℓ is the angle between the direction of μ^- and the direction opposite to $\bar{B}^0$ in the Z' rest frame, θ_K is the angle between the direction of K^- and the direction opposite to $\bar{B}^0$ in the $\bar{K}^{*0}$ rest frame, and ϕ is the angle between the $Z' \to \mu^+\mu^-$ decay plane and the $K^{*0} \to K^-\pi^+$ decay plane in the $\bar{B}^0$ rest frame.

If a new scalar-boson χ mediates the four-body decay instead of the vector-boson Z', the angular distribution simply behaves as $d\Gamma/d\cos\theta_K d\cos\theta_\ell d\phi \propto \cos^2\theta_K$. This is the case assumed in the LHCb search [45] for hidden-sector bosons χ in $B^0 \to K^{*0}\chi$. In order to convert the limits on $B^0 \to K^{*0}\chi$ into the Z' case, one needs to know the ratio of the efficiencies between the χ and Z' cases. The Supplemental Material of Ref. [45] provides this information in the form of the ratio between integrals of the trigonometric functions appearing in Eq. (A1) and integral of $\cos^2\theta_K$, taking into account the efficiency. Using this information, we obtain the ratio of efficiencies for Z' to χ, as shown in Fig. 10. For $g^R_{sb} = 0$, corresponding to the loop-induced coupling discussed in Sec. III, the change in efficiencies from the scalar case is within 6% for

$m_{Z'} \leq 400$ MeV. If we allow a general chiral structure for bsZ' coupling, the change is still small, within 20% for $m_{Z'} \leq 400$ MeV.

APPENDIX B: LOOP FUNCTIONS FOR EFFECTIVE COUPLINGS

The loop functions given in Eq. (45) are approximate formulas in the large-m_U limit. In our numerical study, we use the following expression:

$$f_{qq'} = -4m_W^2 m_U^4 I_0^{qq'} + (2m_W^2 + m_U^2) m_U^2 I_2^{qq'} - 2m_U^2 I_4^{qq'}, \tag{B1}$$

where q, $q' = t$, c, and

$$I_0^{qq'} \equiv \int \frac{d^4k}{i(2\pi)^4} \frac{16\pi^2}{(k^2 - m_q^2)(k^2 - m_{q'}^2)(k^2 - m_U^2)^2(k^2 - m_W^2)} = -\int_0^1 dx_1 \int_0^{1-x_1} dx_2 \frac{(1 - x_1 - x_2)^2}{\alpha_{qq'}\beta_{qq'}^2}, \tag{B2}$$

$$I_2^{qq'} \equiv \int \frac{d^4k}{i(2\pi)^4} \frac{16\pi^2 k^2}{(k^2 - m_q^2)(k^2 - m_{q'}^2)(k^2 - m_U^2)^2(k^2 - m_W^2)} = \frac{2}{(m_U^2 - m_W^2)^2} \int_0^1 dx_1 \int_0^{1-x_1} dx_2 \times \left[\ln \frac{\beta_{qq'}}{\alpha_{qq'}} - \frac{(1 - x_1 - x_2)(m_U^2 - m_W^2)}{\beta_{qq'}} \right], \tag{B3}$$

$$I_4^{qq'} \equiv \int \frac{d^4k}{i(2\pi)^4} \frac{16\pi^2 (k^2)^2}{(k^2 - m_q^2)(k^2 - m_{q'}^2)(k^2 - m_U^2)^2(k^2 - m_W^2)} = -\frac{6}{m_U^2 - m_W^2} \int_0^1 dx_1 \int_0^{1-x_1} dx_2 \times \left(1 - x_1 - x_2 - \frac{\alpha_{qq'}}{m_U^2 - m_W^2} \ln \frac{\beta_{qq'}}{\alpha_{qq'}} \right), \tag{B4}$$

with

$$\alpha_{qq'} = x_1 m_q^2 + x_2 m_{q'}^2 + (1 - x_1 - x_2) m_W^2,$$
$$\beta_{qq'} = x_1 m_q^2 + x_2 m_{q'}^2 + (1 - x_1 - x_2) m_U^2. \tag{B5}$$

[1] K. A. Olive *et al.* (Particle Data Group), Chin. Phys. C **38**, 090001 (2014).
[2] R. Aaij *et al.* (LHCb Collaboration), Phys. Rev. Lett. **111**, 191801 (2013).
[3] LHCb Collaboration, Report No. LHCb-CONF-2015-002.
[4] R. Aaij *et al.* (LHCb Collaboration), Phys. Rev. Lett. **113**, 151601 (2014).
[5] S. Descotes-Genon, J. Matias, and J. Virto, Phys. Rev. D **88**, 074002 (2013).
[6] W. Altmannshofer and D. M. Straub, Eur. Phys. J. C **73**, 2646 (2013).
[7] F. Beaujean, C. Bobeth, and D. van Dyk, Eur. Phys. J. C **74**, 2897 (2014); **74**, 3179(E) (2014).
[8] R. R. Horgan, Z. Liu, S. Meinel, and M. Wingate, Phys. Rev. Lett. **112**, 212003 (2014).
[9] T. Hurth and F. Mahmoudi, J. High Energy Phys. 04 (2014) 097.
[10] R. Alonso, B. Grinstein, and J. M. Camalich, Phys. Rev. Lett. **113**, 241802 (2014).
[11] G. Hiller and M. Schmaltz, Phys. Rev. D **90**, 054014 (2014).
[12] D. Ghosh, M. Nardecchia, and S. A. Renner, J. High Energy Phys. 12 (2014) 131.
[13] T. Hurth, F. Mahmoudi, and S. Neshatpour, J. High Energy Phys. 12 (2014) 053.
[14] W. Altmannshofer and D. M. Straub, Eur. Phys. J. C **75**, 382 (2015).
[15] W. Altmannshofer, S. Gori, M. Pospelov, and I. Yavin, Phys. Rev. D **89**, 095033 (2014).
[16] X.-G. He, G. C. Joshi, H. Lew, and R. R. Volkas, Phys. Rev. D **43**, R22 (1991).
[17] P. J. Fox, J. Liu, D. Tucker-Smith, and N. Weiner, Phys. Rev. D **84**, 115006 (2011).
[18] S. Jung, H. Murayama, A. Pierce, and J. D. Wells, Phys. Rev. D **81**, 015004 (2010).
[19] F. Jegerlehner and A. Nyffeler, Phys. Rep. **477**, 1 (2009).
[20] S. Baek, N. G. Deshpande, X.-G. He, and P. Ko, Phys. Rev. D **64**, 055006 (2001).
[21] W. Altmannshofer, S. Gori, M. Pospelov, and I. Yavin, Phys. Rev. Lett. **113**, 091801 (2014).
[22] K. Fuyuto, W.-S. Hou, and M. Kohda, Phys. Rev. Lett. **114**, 171802 (2015).
[23] Y. Grossman and Y. Nir, Phys. Lett. B **398**, 163 (1997).
[24] T. Araki, F. Kaneko, Y. Konishi, T. Ota, J. Sato, and T. Shimomura, Phys. Rev. D **91**, 037301 (2015).
[25] M. G. Aartsen *et al.* (IceCube Collaboration), Phys. Rev. Lett. **113**, 101101 (2014).
[26] W.-S. Hou and M. Kohda (to be published).
[27] S. R. Mishra *et al.* (CCFR Collaboration), Phys. Rev. Lett. **66**, 3117 (1991).
[28] G. Aad *et al.* (ATLAS Collaboration), Phys. Rev. Lett. **112**, 231806 (2014).
[29] K. Harigaya, T. Igari, M. M. Nojiri, M. Takeuchi, and K. Tobe, J. High Energy Phys. 03 (2014) 105.
[30] A. Crivellin, G. D'Ambrosio, and J. Heeck, Phys. Rev. Lett. **114**, 151801 (2015).

[31] G. Aad *et al.* (ATLAS Collaboration), Eur. Phys. J. C **76**, 12 (2016).
[32] S. Chatrchyan *et al.* (CMS Collaboration), Phys. Rev. Lett. **112**, 171802 (2014).
[33] CMS Collaboration, Report No. CMS-PAS-FTR-13-016.
[34] CMS Collaboration, arXiv:1307.7135.
[35] S. Chatrchyan *et al.* (CMS Collaboration), Phys. Lett. B **718**, 1252 (2013).
[36] ATLAS Collaboration, arXiv:1307.7292.
[37] K. Agashe *et al.* (Top Quark Working Group Collaboration), arXiv:1311.2028.
[38] L.-B. Jia, Phys. Rev. D **92**, 074006 (2015).
[39] J. D'Hondt, A. Mariotti, K. Mawatari, S. Moortgat, P. Tziveloglou, and G. Van Onsem, arXiv:1511.07463.
[40] S. Oh and J. Tandean, J. High Energy Phys. 01 (2010) 022.
[41] P. Ball and R. Zwicky, Phys. Rev. D **71**, 014015 (2005).
[42] P. Ball and R. Zwicky, Phys. Rev. D **71**, 014029 (2005).
[43] M. Beneke, T. Feldmann, and D. Seidel, Nucl. Phys. **B612**, 25 (2001).
[44] M. Williams, J. Instrum. **10**, P06002 (2015).
[45] R. Aaij *et al.* (LHCb Collaboration), Phys. Rev. Lett. **115**, 161802 (2015).
[46] H. J. Hyun *et al.* (Belle Collaboration), Phys. Rev. Lett. **105**, 091801 (2010).
[47] R. Aaij *et al.* (LHCb Collaboration), J. High Energy Phys. 02 (2013) 105.
[48] R. Aaij *et al.* (LHCb Collaboration), J. High Energy Phys. 06 (2014) 133.
[49] J. P. Lees *et al.* (*BABAR* Collaboration), Phys. Rev. D **87**, 112005 (2013).
[50] O. Lutz *et al.* (Belle Collaboration), Phys. Rev. D **87**, 111103 (2013).
[51] R. Aaij *et al.* (LHCb Collaboration), J. High Energy Phys. 12 (2012) 125.
[52] R. Aaij *et al.* (LHCb Collaboration), J. High Energy Phys. 10 (2015) 034.
[53] F. Mescia and C. Smith, Phys. Rev. D **76**, 034017 (2007).
[54] G. Ecker, A. Pich, and E. de Rafael, Nucl. Phys. **B291**, 692 (1987).
[55] J. R. Batley *et al.* (NA48/2 Collaboration), Phys. Lett. B **697**, 107 (2011).
[56] A. Alavi-Harati *et al.* (KTeV Collaboration), Phys. Rev. Lett. **84**, 5279 (2000).
[57] P. Mertens and C. Smith, J. High Energy Phys. 08 (2011) 069.
[58] J. R. Batley *et al.* (NA48/1 Collaboration), Phys. Lett. B **599**, 197 (2004).
[59] A. V. Artamonov *et al.* (E949 Collaboration), Phys. Rev. Lett. **101**, 191802 (2008).
[60] A. V. Artamonov *et al.* (E949 Collaboration), Phys. Rev. D **79**, 092004 (2009).
[61] A. V. Artamonov *et al.* (E949 Collaboration), Phys. Rev. D **72**, 091102 (2005).
[62] J. K. Ahn *et al.* (E391a Collaboration), Phys. Rev. D **81**, 072004 (2010).
[63] T. Araki, F. Kaneko, T. Ota, J. Sato, and T. Shimomura, Phys. Rev. D **93**, 013014 (2016).
[64] http://na62.web.cern.ch/na62/.
[65] http://koto.kek.jp/.
[66] K. Shiomi, $K_L \to \pi^0 \nu\bar{\nu}$ at KOTO, in *Proceeding of the 8th International Workshop on the CKM Unitarity Triangle (CKM2014) Vienna, Austria*, 2014 [arXiv: 1411.4250].
[67] H. K. Dreiner, S. Grab, D. Koschade, M. Kramer, B. O'Leary, and U. Langenfeld, Phys. Rev. D **80**, 035018 (2009).
[68] J. de Vries, H. K. Dreiner, and D. Schmeier, arXiv:1511.07436.
[69] http://lbne.fnal.gov/.
[70] R. Aaij *et al.* (LHCb Collaboration), J. High Energy Phys. 08 (2013) 131.